



UNIVERSITÀ POLITECNICA DELLE MARCHE
Repository ISTITUZIONALE

Influence of viscous dampers ultimate capacity on the seismic reliability of building structures

This is the peer reviewed version of the following article:

Original

Influence of viscous dampers ultimate capacity on the seismic reliability of building structures / Scozzese, Fabrizio; Gioiella, Laura; Dall'Asta, Andrea; Ragni, Laura; Tubaldi, Enrico. - In: STRUCTURAL SAFETY. - ISSN 0167-4730. - 91:(2021). [10.1016/j.strusafe.2021.102096]

Availability:

This version is available at: 11566/299441 since: 2024-04-27T16:51:45Z

Publisher:

Published

DOI:10.1016/j.strusafe.2021.102096

Terms of use:

The terms and conditions for the reuse of this version of the manuscript are specified in the publishing policy. The use of copyrighted works requires the consent of the rights' holder (author or publisher). Works made available under a Creative Commons license or a Publisher's custom-made license can be used according to the terms and conditions contained therein. See editor's website for further information and terms and conditions.

This item was downloaded from IRIS Università Politecnica delle Marche (<https://iris.univpm.it>). When citing, please refer to the published version.

(Article begins on next page)

Influence of viscous dampers ultimate capacity on the seismic reliability of building structures

Fabrizio Scozzese ^a, Laura Gioiella ^a, Andrea Dall'Asta ^a, Laura Ragni ^b, Enrico Tubaldi ^c

^a SAAD, University of Camerino, Viale della Rimembranza 3, 63100 Ascoli Piceno, Italy

^b Department of Civil and Building Engineering and Architecture, Università Politecnica delle Marche, Via Brecce Bianche, 60131 Ancona, Italy

^c Department of Civil and Environmental Engineering, University of Strathclyde 75 Montrose Street, Glasgow G1 1XJ, UK

ABSTRACT

Anti-seismic devices should be designed with proper safety margins against their failure, because the reliability of the structural system where they are installed is strongly influenced by their reliability. Seismic standards generally prescribe safety factors (reliability factors) amplifying the device responses at the design condition, in order to reach a target safety level. In the case of Fluid Viscous Dampers (FVDs), these factors are applied to the stroke and velocity, and their values are not homogenous among seismic codes.

This paper investigates the influence of the values of the safety factors for FVDs on the reliability of the devices and of the structural systems equipped with them. An advanced FVD model is employed to account for the impact forces arising when the dampers reach the end-stroke and the brittle failure due to the attainment of the maximum force capacity. The effect of damper failure on both the fragility and the seismic risk of the structural system is investigated by performing multiple-stripe analysis and monitoring different global and local demand parameters. In particular, a parametric study has been carried out, considering two case studies consisting of a low-rise and a medium-rise steel building, coupled with a dissipative system with linear and nonlinear properties and studying the consequences of different values of safety factors for stroke and forces. The study results give evidence to the potential brittle behaviour of the coupled system and provide information about the relationships between damper safety factors and effective structural reliability. Some preliminary suggestions are given on possible improvements of current design approaches and on the values of the reliability factors to be considered for future code revision.

Keywords: energy dissipation; failure; seismic risk and safety; reliability factors; multiple stripe analysis; nonlinear dynamic analysis.

28 1 INTRODUCTION

29 Fluid viscous dampers (FVDs) are devices widely used for seismic passive protection of both new
30 and existing structures. They are widely employed for reducing displacements and interstorey drift
31 demands in newly-designed structures as well as in existing ones by using both external and internal
32 configurations [1]-[8].

33 Several approaches are to date available for designing both size and location of viscous dampers
34 within a building frame based on direct procedures [1][9][10][11][12] or optimization methods
35 [13][14] (see [15] for a thorough review of design strategies for viscous dampers). These design
36 approaches generally allow to control the seismic performance of buildings under the design seismic
37 intensity level. However, the reliability under extreme, low-probability earthquake events may be
38 characterized by low robustness and inadequate safety levels because dampers usually exhibit a brittle
39 collapse behaviour and their failure may trigger the collapse of the whole system. Consequently, the
40 choice of adequate safety factors for the design of the dampers is of paramount importance for
41 obtaining a satisfactory performance under strong actions and controlling the probability of failure.

42 It is noteworthy that the robustness under extreme loadings is usually not a concern for traditional
43 steel and concrete structures, thanks to their redundant static schemes and ductile material properties,
44 able to redistribute the structural damage. Thus, frame structures generally behave well under
45 exceptional actions, provided that details or connections are adequately designed [16][17][18].
46 Moreover, procedures to make high quality structural components are consolidated as well as safety
47 coefficients to be used in the design. As a result, while code conforming traditional solutions are
48 characterized by adequate reliability levels, code conforming structures equipped with fluid viscous
49 dampers may show reliability levels below the target suggested by the design codes and the technical
50 literature [19][20][21][22][23].

51 In order to evaluate the probability of collapse of structures equipped with dampers, risk analyses
52 must be performed by using probabilistic approaches [24]-[32]. Recent probabilistic analyses have
53 investigated some specific issues, such as the effect of ground motion variability on the response of
54 systems equipped with either linear and nonlinear viscous dampers [27][28][29]; the influence of the
55 degree of nonlinearity of the dampers [28][30], and the effect of the damper parameters variability
56 [30][31][32] stemming from the device manufacturing process, as acknowledged by the main
57 international Standards for seismic structural design [19][20][21][22]. However, in these studies the
58 device failure was not explicitly taken into account. Thus, more accurate studies simulating the effect
59 of the device failure should be carried out to provide a better evaluation of the structural reliability
60 under strong earthquakes.

61 This paper aims to evaluate the consequences of the dissipative device failure on the seismic
62 performance of two benchmark structural systems, by adopting a model describing the brittle failure
63 of the devices due to the attainment of the force capacity, related to the over-velocity or to the
64 achievement of the end-stroke and its influence on the structural reliability. In particular, it is assumed
65 that a brittle failure occurs in the dampers once the maximum force is attained, consistently with the
66 viscous damper numerical model proposed in [33]. The problem is analysed by using a probabilistic
67 approach and by evaluating the mean annual frequency of exceedance of different values of the
68 multiple response parameters related to the performance of dampers and structure. For this purpose,
69 Multi Stripe Analysis (MSA) [34] is carried out and results are given in terms of fragility curves and
70 demand hazard curves for the engineering demand parameters (EDPs) of interest. Fragility analyses
71 of failure of dampers give evidence to the failure sequence and potential lack of robustness of the
72 coupled system.

73 The two case studies analysed here consist of steel buildings with different dynamic properties,
74 already considered as benchmark cases in previous studies (SAC Phase II Steel Project, [42]). For
75 consistency with the adopted benchmark case studies, the seismic hazard is also assumed equal to the
76 one of [42]. The dissipative system is dimensioned to provide an added damping equal to 30%, using
77 both linear and nonlinear devices, by varying their degree of nonlinearity among three values. The

78 capacity of the dampers (stroke and strength) is evaluated at the design condition, corresponding to a
79 seismic action with Mean Annual Frequency (MAF) of exceeding equal to 2×10^{-3} .

80 Some preliminary results under increasing harmonic load histories are reported to illustrate the
81 model capabilities and the sequence of failures triggered by the damper failure. Subsequently,
82 fragility curves and demand hazard curves are illustrated, where the structural performance is
83 analysed considering MAF of exceeding up to 10^{-5} 1/yr. Results obtained by considering different
84 amplification factors for the design of damper parameters are evaluated and compared. In particular,
85 the prescriptions of European codes [20][21] and American Standards [19] are considered. Parametric
86 analysis includes both the case of linear viscous dampers and nonlinear viscous dampers with
87 different nonlinear properties. The case without dampers and the one in which the damper failure is
88 disregarded are also considered for comparison purposes.

89 The obtained results shed light on the influence of the damper failure on the global reliability of
90 the system and on the effect of the amplification factors on the MAF of failure.

91 2 FVDS MODELLING AND SEISMIC CODE PROVISIONS

92 2.1 Fluid viscous dampers modelling

93 The constitutive law of a fluid viscous damper (FVD) can be described through the following
94 relationship [33][43]:

$$F_d(v) = c|v|^\alpha \text{sgn}(v) \quad (1)$$

95 where v is the relative velocity between the device ends, F_d is the damper resisting force, $|v|$ is
96 the absolute value of v , sgn is the sign operator, c and α are two constitutive parameters: the former
97 is an amplification factor, while the latter describes the damper nonlinear behaviour.

98 It is worth noting that viscous dampers can be produced with α values ranging from 0.1 and 2.
99 Devices with $\alpha > 1$ are not dissipative and are used as shock transmitters. Devices with $0.1 \leq \alpha \leq 1.0$
100 are all potentially suitable for seismic energy dissipation, among these values, the range $0.3 \leq \alpha \leq 1.0$
101 is the most widespread [35][36][37][38].

102 A fluid viscous damper generally consists of a steel cylinder filled of a silicone fluid, within which
103 a steel piston with small orifices on its head can move. In case of seismic events, the fluid is forced
104 to pass through the orifices, moving from one side to the opposite side of the cylinder, thus dissipating
105 into heat the input mechanical energy. The higher is the velocity of the movement, the greater is the
106 dissipated energy. The cylinder is equipped with spherical hinges at its ends to avoid device bending.
107 FVDs are generally connected to the structure by a stiff connection, consisting in a driver brace,
108 dimensioned using an over-strength factor with respect to the viscous device. The stiffness of the
109 driver brace is an important feature, because it needs to be sufficiently high to allow the device to be
110 effective in dissipating energy. Further details on the damper components and their behaviour can be
111 found in [33].

112 The failure of a damper is related to the exceedance of its strength capacity and can be attained
113 because of the forces related to the end-stroke impact or can be due to excessive piston velocity.
114 According to the described behaviour, dampers are generally classified and tested with reference to
115 two characteristic parameters: the maximum values of stroke $\Delta_{d,max}$, and the maximum transmissible
116 force $F_{d,max}$.

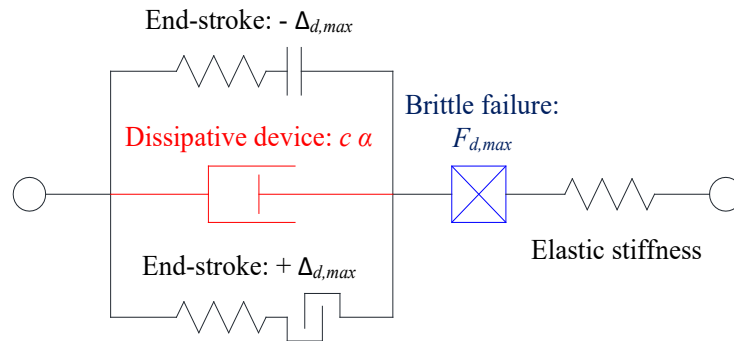
117 The end-stroke can be attained both in tension (maximum elongation of the device) and in
118 compression (maximum shortening of the device). However, the attainment of an impact does not
119 strictly imply the damper failure because the impact force may be lower than the device strength.

120 The second mechanism refers to the attainment of the maximum viscous force due to an excessive
121 value of the velocity of the piston (over-velocity with respect to the design value). This extreme value
122 of the force can induce a leak of the fluid or can damage the damper components, resulting in the
123 failure of the device. It is noteworthy that once the maximum capacity ($F_{d,max}$) is attained, the

124 resulting failure mechanisms is brittle, thus making the device ineffective, with no residual ability to
 125 sustain loads or dissipate energy.

126 The model, proposed hereinafter, aims to describe the two aforesaid mechanisms using the damper
 127 model, depicted in **Fig. 1**. It is composed of three elements: a dashpot, describing the dissipative
 128 behaviour; a hook and gap element, set in parallel to the dissipative device, which simulate the impact
 129 due to either excessive shortening ($-\Delta_{d,max}$) or elongation ($+\Delta_{d,max}$); and a third element, set in
 130 series with the others, simulating the failure due to the attainment of the force capacity. In this paper,
 131 the strength capacity is assumed to be the same in traction and in compression and the failure occurs
 132 when the modulus of damper force attains the limit value $F_{d,max}$.

133 The damper model discussed above is implemented in OpenSees [44] using two-node link
 134 elements simulating each of the three components, while various material properties are used to
 135 describe the different behaviours. A “Viscous material” is used for the dissipative element, by
 136 assigning the values of the constitutive parameters c and α . An “ElasticMultilinear material” depicts
 137 the force-displacement relationship related to impacts occurring both for elongation and shortening.
 138 Finally, a “MinMax material” is used to simulate the brittle failure, assigning the value of the strength
 139 capacity $F_{d,max}$. The stiffness of the “MinMax material” can be used to model the overall
 140 deformability of damper, connections, and brace. However, once the strength capacity is reached, the
 141 element fails and does not provide any more contribution in terms of reaction force.



142

143

Fig. 1. Dissipative device model encompassing the failure mechanisms

144 *2.2 International regulatory framework: an overview*

145 Modern seismic codes prescribe that anti-seismic devices shall be dimensioned starting from the
 146 values of the control parameters evaluated for seismic design actions having an assigned probability
 147 of exceedance. Then, the capacities of the devices are assigned amplifying these control parameters,
 148 which are stroke and force for the FVDs, by means of amplification factors, or reliability factors, in
 149 order to ensure a target level of safety. This procedure makes simpler the dimensioning, avoiding an
 150 explicit probabilistic analysis considering all the uncertainties of interest. Generally, in the case of
 151 dampers, Standards suggest reliability factors that account for uncertainties related to damper
 152 response, manufacturing tolerances, ageing phenomena and temperature variations, in addition to
 153 uncertainties related to seismic action and structure.

154 The amplification factors proposed by Codes are two and aim to control the two failure
 155 mechanisms discussed above. The former, here denoted by γ_{Δ} , amplifies the maximum stroke
 156 measured at design condition. The amplified stroke must not exceed the damper capacity $\Delta_{d,max}$. The
 157 latter, here denoted by γ_v , amplifies the maximum velocity measured at design condition. Damper
 158 force is obtained by Eqn. (1) and must not exceed the damper capacity $F_{d,max}$.

159 In this study we refer to the provisions of US and EU Codes. In the US, the standard for the retrofit
 160 of existing buildings (ASCE 41-2017) [19] provides clear indications on the values and applicability
 161 of safety factors for viscous dampers. It prescribes that all energy dissipation devices shall be capable
 162 of sustaining the force and displacement associated with a velocity equal to 130% ($\gamma_{\Delta} = \gamma_v = 1.3$)
 163 or 200% ($\gamma_{\Delta} = \gamma_v = 2.0$) of the maximum calculated velocity for that device. The two options

164 depend on the number of devices installed within each storey and each direction of the building and
165 the performance objective assumed [19]. The safety coefficients should be applied to the velocity
166 calculated with a seismic action characterized by an exceedance probability of 5% in 50 years for
167 existing buildings or the Risk-Targeted Maximum Considered Earthquake (MCE) [22] for the new
168 ones. The value of 200% applies only in the case that less than four energy dissipation devices are
169 installed in a given storey along one principal direction of the building, otherwise the coefficient
170 130% can be used. In the ASCE 41-2017 [19] the property variations of the energy dissipation devices
171 are taken into account through the so called property modification factors (λ factors). These factors
172 define the upper- and lower-bound properties of the devices, accounting for manufacturing tolerances,
173 device characteristics not explicitly considered during testing and environmental effects and aging.
174 The λ factors are not considered in the present work.

175 In Europe, the reference standards are Eurocode 8 [21] and EN15129 [20], which regulates the
176 devices production and integrates the Eurocode prescriptions concerning design and structural
177 reliability. In the section "General design rules" of EN15129, it is specified that, for anti-seismic
178 devices (seismic isolators excluded), a reliability factor γ_x equal or greater than 1 shall be applied to
179 the effects of the design seismic action on the devices, while an over-strength factor $\gamma_{Rd} = 1.1$ is
180 recommended for designing the connections with the structure. According to Eurocode 8, the design
181 seismic action shall be evaluated considering the Ultimate Limit State (ULS) hazard intensity,
182 characterized by an exceedance probability of 10% in 50 years, corresponding to a MAF of
183 exceedance equal to 2.1×10^{-3} . The value of the reliability factor should be provided by the Eurocodes
184 (as specified in section 4.1.2, note 2 of EN15129), but this information is lacking in the current
185 version. The same EN15129, in the section dedicated to velocity dependent devices, prescribes that
186 the design velocity shall be amplified by a reliability factor $\gamma_v = 1.5$. However, it is worth to observe
187 that no amplification factor is specified for the damper stroke, which means that the stroke capacity
188 could be determined by assuming a γ_Δ factor equal to 1.0. The Italian standard, NTC 2018 [45], is
189 compatible with European codes but its prescriptions are more demanding, requiring that design
190 velocities are amplified by the same reliability factor γ_v given by the EN15129, but prescribes that
191 the response parameters of the devices are evaluated at the Collapse Limit State (seismic actions with
192 exceedance probability of 5% in 50 years). However, similarly to EN15129, no specific indications
193 are given about the damper stroke capacity. Similarly to the US Code [19], also the EN15129 provides
194 tolerance limits (t_d) for velocity dependent devices which are relevant to variations within the supply
195 (statistical variations), as well as variations due to temperature, ageing, etc. These indications
196 regarding the tolerances are also adopted by the Italian NTC 2018 [45] and are not considered in this
197 work.

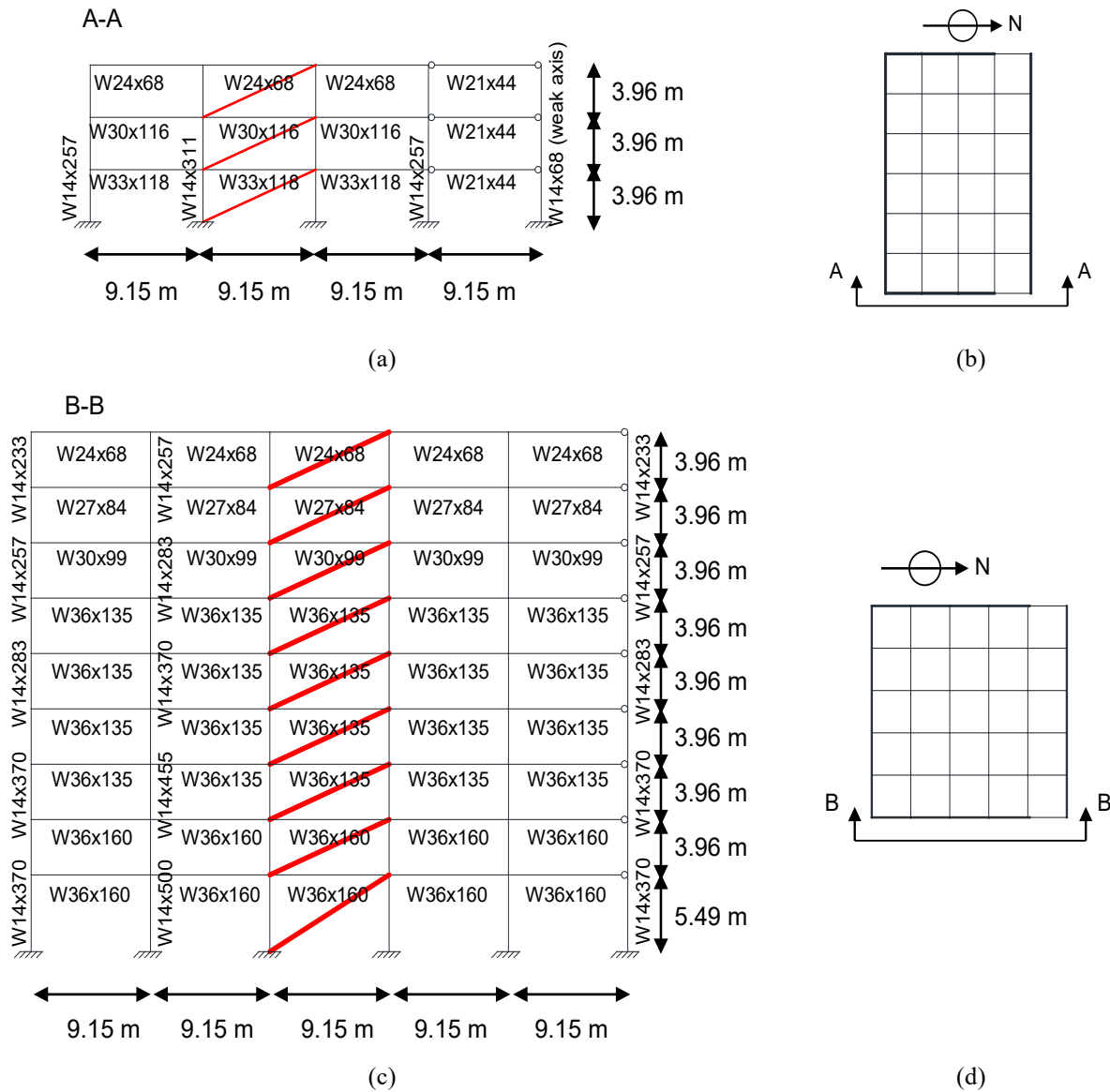
198 3 PARAMETRIC ANALYSIS

199 In this section, a parametric analysis is carried out to understand how the failure of dampers affects
200 the seismic response and performance of steel frame structures. Two different steel moment-resisting
201 frames are considered, representative of low-rise and medium-rise building. The buildings are
202 equipped with FVDs with different non-linearity levels, corresponding to values of the damper
203 exponent α of 1.0, 0.6 and 0.3. Different values of the amplification factors are considered for
204 dampers design. The obtained results are also compared to those corresponding to two limit cases: a)
205 without dampers (bare frame), and b) dampers do not fail.

206 3.1 Steel buildings frame structures

207 The two case studies consist of a 3-storey and 9-storey steel moment-resisting frame buildings,
208 designed as part of the SAC Phase II Steel Project, and located in the Los Angeles area. The buildings
209 were designed for gravity, wind, and seismic loads in order to conform to local code requirements
210 and have been widely used as benchmark structure in several studies concerning structural response
211 control (e.g., [2][42][28][46]). **Fig. 2** illustrates the structural system of the buildings, consisting of

212 perimeter moment-resisting frames and internal gravity frames with shear connections. The numerical
 213 model of the buildings consists only in a two-dimensional frame, representing one half of the structure
 214 in the north–south direction, which is the short and also the weak direction of the buildings. **Fig. 2**
 215 also shows the main geometrical details and dimensions of the steel members (wide-flange sections
 216 are used for both columns and beams), together with the locations of the fluid viscous dampers, whose
 217 design is described in section 3.3. Further details concerning the structural geometry and loads can
 218 be found in [46].



219 **Fig. 2.** Case studies: (a) elevation (red lines highlight FVDs location) and (b) plan (thick lines
 220 highlight moment-resisting frames) of 3-storey frame; (c) elevation and (d) plan of 9-storey frame.

221 The finite element models of the systems are developed in OpenSees [44] following the same
 222 methodology described in [28] and briefly recalled below. A distributed plasticity approach is adopted
 223 [47][48], with nonlinear force-based elements and fibre sections with *Steel02* uniaxial material,
 224 accounting for the hysteretic behaviour of the members. A corotational approach for the system
 225 coordinate transformation is used to perform large displacement (small strain) analysis and thus
 226 account for the nonlinear geometrical effects, whereas an elastic fictitious P-delta column is
 227 introduced to consider the vertical loads carried by the inner gravity frames (not explicitly modelled).
 228 The strength and deformability of panel zones are neglected. The inherent damping properties are
 229 accounted through the Rayleigh model by assigning a 2% damping ratio at the first and second
 230 vibration modes. **Table 1** reports, for both the bare buildings, the first three estimated vibration

231 periods T_i , together with the related mass participant factors normalized with respect to the total mass,
 232 (MPF_i).

233

234

Table 1. Vibration periods for the bare 3-storey and 9-storey steel moment-resisting frame.

3-storey case study			9-storey case study		
Mode	T_i [s]	MPF_i	Mode	T_i [s]	MPF_i
1	0.995	0.827	1	2.225	0.828
2	0.325	0.136	2	0.836	0.109
3	0.173	0.037	3	0.481	0.038

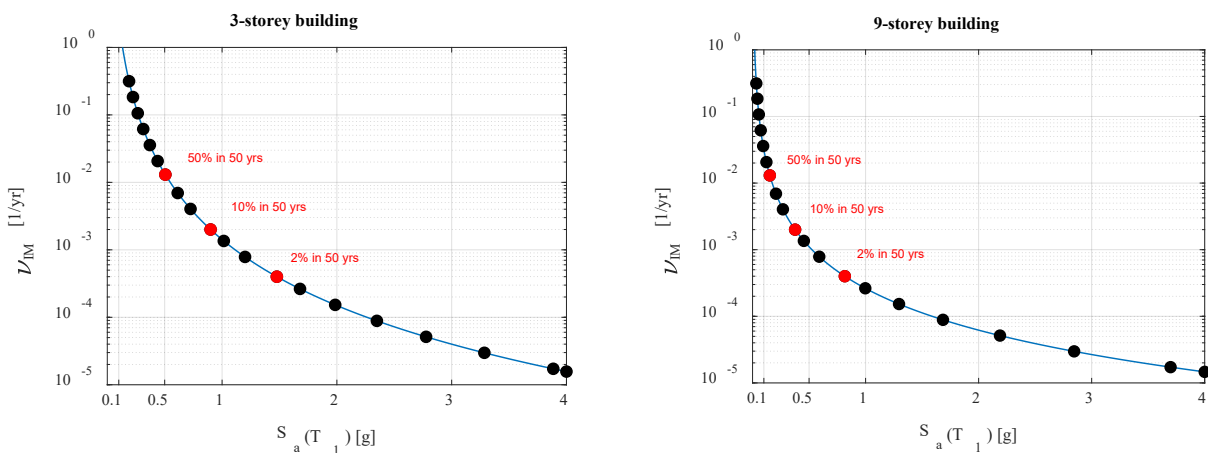
235 **3.2 Seismic hazard**

236 For consistency with the adopted benchmark case studies, the seismic hazard is based on [42]. The
 237 spectral pseudo-acceleration $S_a(T_1)$ of a linear elastic SDOF system with 2% damping ratio and
 238 fundamental vibration period equal to that of the structure T_1 is considered as intensity measure (IM).
 239 Such IM also represents the basis of the current seismic hazard maps and building code practice [49].
 240 **Fig. 3** illustrates the hazard curves corresponding to the chosen IM , for the three-storey and the nine-
 241 storey building frames. The IM levels at which MSA is performed are 20 (highlighted by circles in
 242 **Fig. 3**), whose corresponding values of spectral accelerations are summarised in **Table 2**. The IM
 243 values corresponding to the main limit states suggested by codes are identified by red circles, and
 244 they correspond to seismic events with exceedance probability of 50%, 10% and 2% in 50 years.

245 The record-to-record variability effects are taken into account in the analyses by considering the
 246 set of 60 records used in the SAC project [2]. These records are characterized by different seismic
 247 intensities, frequency content, and duration. At each intensity level, a subset of 30 ground motions is
 248 taken from this set, with IM values closest to the considered IM level, in order to minimize the scaling
 249 procedure operated for making the samples conditional to the IM . Further details and features of these
 250 records can be found in [2].

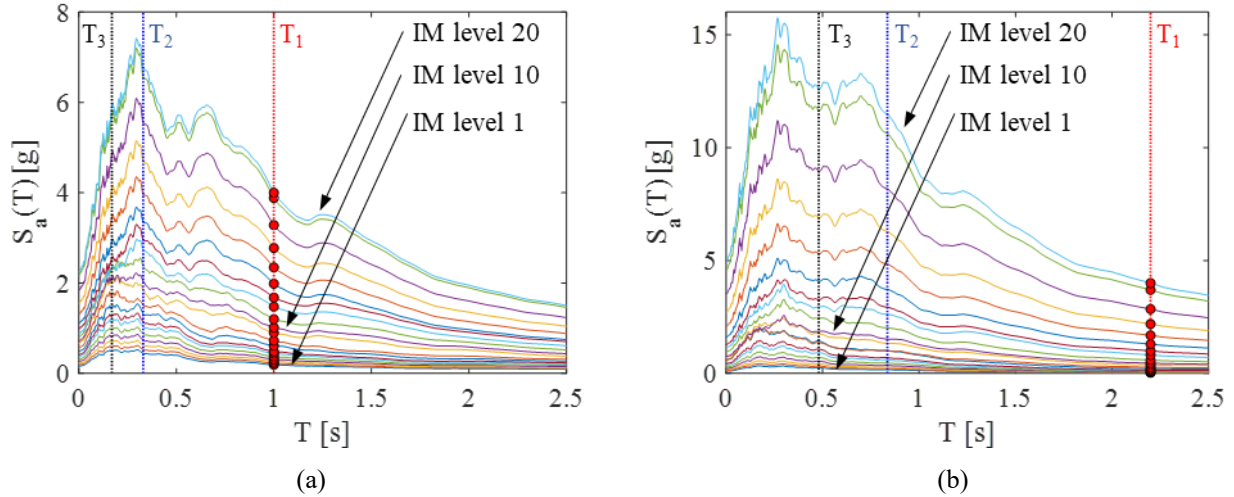
251 For what concerns the FVDs design, this is carried out by considering the set of 30 records
 252 corresponding to a MAF of exceedance $\nu_{design} = \nu_{IM}(im_{design}) = 0.0021$ 1/yr (probability of exceedance
 253 of 10% in 50 years), associated to the intensities $im_{design} = 0.8866$ g for the three-storey frame and
 254 $im_{design} = 0.3676$ g for the nine-storey frame (g is the gravity acceleration).

255



256

Fig. 3. IM hazard curves for the 3- and 9-storey buildings.



257 **Fig. 4.** Ground motion response spectra averaged at every intensity level: (a) 3-storey; (b) 9-storey.

258 **Table 2.** Correspondence between IM levels and spectral accelerations (in g).

IM levels	1	2	3	4	5	6	7	8	9	10
3-storey $S_a(T_1=1.0)$	0.19	0.22	0.27	0.31	0.37	0.44	0.48	0.61	0.73	0.90
9-storey $S_a(T_1=2.2)$	0.03	0.04	0.06	0.07	0.09	0.12	0.14	0.21	0.27	0.38
IM levels	11	12	13	14	15	16	17	18	19	20
3-storey $S_a(T_1=1.0)$	1.01	1.20	1.48	1.68	1.99	2.35	2.78	3.28	3.89	4.00
9-storey $S_a(T_1=2.2)$	0.45	0.59	0.82	1.00	1.30	1.68	2.19	2.85	3.70	4.00

259

260 3.3 Damping systems

261 The design of the FVDs is carried out to enhance the buildings performance under a seismic
 262 scenario with a 10% probability of exceedance in 50 years (ULS scenario according to Eurocode 8).
 263 To this aim, a target value $\xi_{add} = 30\%$ has been chosen for supplemental damping. It is worth noting
 264 that a damping ratio higher than 30% is usually not recommended because it may lead to a too
 265 significant modification of the natural dynamic properties of the building, with potentially detrimental
 266 effects in terms of absolute accelerations ([2][15][50]). For this reason, the value of 30% is assumed
 267 to investigate an upper bound of the retrofitting scenarios with passive seismic protection strategies.
 268 This value is expected to lead to the worst consequences in case of dampers failure.

269 Dampers design is initiated under the hypothesis of linear viscous behaviour ($\alpha = 1.0$); constants
 270 c_j required to achieve the target damping ratio ξ_{add} are thus calculated for each building storey using
 271 the general formula proposed by the ASCE/SEI-41 [19]:

$$\xi_{add} = \frac{T \sum_j c_j f_j^2 \phi_{rj}^2}{4\pi \sum_i m_i \phi_i^2} \quad (2)$$

272 where the index $j = 1, \dots, n$ denotes the j -th device, T is the period of the first vibration mode of
 273 the building; f_j is a magnification factor related to the installation scheme of dampers; ϕ_{rj} the first
 274 modal relative displacement between the ends of the damper j in the horizontal direction; m_i is the
 275 mass of the i -th storey and ϕ_i is the horizontal first modal displacements of the i -th storey.

276 In the present study, the dampers are installed in a diagonal arrangement, therefore $f_j = \cos\theta$, where
 277 θ is the angle between the horizontal direction and the j -th diagonal brace. Moreover, the damping
 278 coefficients of the linear devices have been distributed proportionally to the storey shear force of the
 279 first mode of the bare frame. As suggested in [9], the relation between the damping coefficient of a
 280 single storey, c_j , and the total damping of the building, $\sum_i c_i$ can be expressed as:

$$c_j = \left(V_j / \sum_i V_i \right) \sum_i c_i \quad (3)$$

281 where V_j is the shear force of the j -th storey. By substituting Eqn. (3) into Eqn. (2), it is possible
282 to achieve the total supplemental damping ξ_{add} as:

$$\xi_{add} = \frac{T \sum_j \left[V_j (\sum_i c_i) (\cos \theta_j \phi_{rj})^2 \right]}{4\pi (\sum_i m_i \phi_i^2) (\sum_i V_i)} \quad (4)$$

283 Eqn. (4) can be rearranged to find the total damping coefficient of the structure, $\sum_i c_i$, and the
284 damping coefficient at the j -th storey can be finally expressed as:

$$c_j = \frac{4\pi \xi_{add} V_j \sum_i m_i \phi_i^2}{T \sum_i V_i (\cos \theta_i \phi_{ri})^2} \quad (5)$$

285 Having determined the damping coefficients of the devices for the linear case, the viscous
286 coefficients for the nonlinear FVD corresponding to given value of the exponent α , are evaluated
287 following the approach outlined in [9],[51],[52] and based on the equivalence of the energies
288 dissipated by the linear and nonlinear FVDs. For this purpose, seismic analyses of the system with
289 linear devices are carried out under a set of 30 recorded ground motions, scaled to the design intensity
290 level (i.e., exceedance probability of 10% in 50 years) as discussed in the previous chapter. The mean
291 response in terms of roof displacement of the building, A , is then used to determine the equivalent
292 nonlinear damping coefficients through the following general expression:

$$\xi_{add} = \frac{T^{2-\alpha} \sum_j c_j \lambda f_j^{1+\alpha} \phi_{rj}^{1+\alpha}}{(2\pi)^{3-\alpha} A^{1-\alpha} \sum_i m_i \phi_i^2} \quad (6)$$

293 where ϕ_i is the modal displacement shape normalised to a unit value at the roof and λ is given by
294 the following expression:

$$\lambda = 2^{2+\alpha} \frac{\Gamma^2(1 + \alpha/2)}{\Gamma(2 + \alpha)} \quad (7)$$

295 in which Γ is the gamma function.

296 Eqn. (6) can be specialized to the case of dampers with viscous constant distributed proportionally
297 to the storey shear force of the first mode of the bare frame, installed in a diagonal arrangement. It
298 can be then rearranged to obtain the nonlinear damping coefficient c_j at each elevation, as:

$$c_j = \frac{\xi_{add} (2\pi)^{3-\alpha} A^{1-\alpha} V_j \sum_i m_i \phi_i^2}{T^{2-\alpha} \sum_i V_i \lambda \cos \theta_i^{1+\alpha} \phi_{ri}^{1+\alpha}} \quad (8)$$

299 **Table 3** and **Table 4** report the properties of the dissipative devices, c_j and α , for the 3-storey and
300 9-storey buildings, respectively, for the various levels of dampers nonlinearity considered. It is
301 noteworthy that the maximum interstorey drift along the building height, averaged over the 30 records
302 considered, is equal to 3% and 2.1% respectively for the three-storey and nine-storey bare frames.
303 With the addition of the dampers, they become respectively 1.2% and 1.0%.

304 **Table 5** and **Table 6** report the values of mean displacement $\Delta_{d,j}$, force $F_{d,j}$ and velocity v_j
305 demand for the dampers, evaluated at the design condition. These values result in a probability of
306 failure of the dampers of about 50% under the design earthquake level, if no amplification factors are
307 considered for the damper response parameters.
308

309

310

311

Table 3. 3-storey building damping properties for different levels of damper nonlinearity.

Case study	α	Floor 1	Floor 2	Floor 3
		c_1	c_2	c_3
$[kNs^\alpha/m^\alpha]$				
3-storey	1	13,780	11,914	7428
	0.6	7477	6465	4031
	0.3	4669	4037	2517

312

313

Table 4. 9-storey building damping properties for different levels of damper nonlinearity.

Case study	α	Floor 1	Floor 2	Floor 3	Floor 4	Floor 5	Floor 6	Floor 7	Floor 8	Floor 9
		c_1	c_2	c_3	c_4	c_5	c_6	c_7	c_8	c_9
$[kNs^\alpha/m^\alpha]$										
9-storey	1	48,103	46,834	44,578	41,282	36,918	31,534	25,199	17,903	9675
	0.6	17,506	17,044	16,233	15,024	13,435	11,476	9171	6515	3521
	0.3	8133	7899	7518	6962	6226	5318	4250	3019	1632

314

315

316

Table 5. 3-storey building damper design parameters at the design condition.

3-storey building									
α	Floor 1	Floor 2	Floor 3	Floor 1	Floor 2	Floor 3	Floor 1	Floor 2	Floor 3
	$\Delta_{d,1}$ [mm]	$\Delta_{d,2}$ [mm]	$\Delta_{d,3}$ [mm]	$F_{d,1}$ [kN]	$F_{d,2}$ [kN]	$F_{d,3}$ [kN]	v_1 [m/s]	v_2 [m/s]	v_3 [m/s]
1.0	35.4	44.5	37.1	3109	3336	1956	0.23	0.28	0.26
0.6	32.4	41.7	35.6	3090	3050	1824	0.23	0.29	0.27
0.3	29.6	39.7	35.7	3044	2796	1712	0.24	0.29	0.28

317

318

Table 6. 9-storey building building damper design parameters at the design condition.

9-storey building										
	Floor 1	Floor 2	Floor 3	Floor 4	Floor 5	Floor 6	Floor 7	Floor 8	Floor 9	
$\alpha=1$	$\Delta_{d,j}$ [mm]	38.4	32.7	31.9	31.9	29.5	27.8	28.7	29.9	24.3
	$F_{d,j}$ [kN]	7781	6060	5416	5075	4379	3930	3559	3011	1614
	v_j [m/s]	0.16	0.13	0.12	0.12	0.12	0.12	0.14	0.17	0.17
$\alpha=0.6$	$\Delta_{d,j}$ [mm]	38.4	32.3	31.0	31.3	28.3	26.6	28.9	30.2	24.4
	$F_{d,j}$ [kN]	6580	5461	4900	4571	3914	3385	3016	2370	1307
	v_j [m/s]	0.20	0.15	0.14	0.14	0.13	0.13	0.16	0.19	0.19
$\alpha=0.3$	$\Delta_{d,j}$ [mm]	38.7	32.4	31.3	30.8	28.7	26.1	29.1	31.0	25.8
	$F_{d,j}$ [kN]	5244	4688	4345	4014	3546	2952	2507	1920	1062
	v_j [m/s]	0.23	0.18	0.16	0.16	0.15	0.14	0.17	0.22	0.24

319

320 3.4 Amplification factors

321 Per each value of the constitutive parameter α and per each case-study, five combinations of
322 amplification factors relevant to damper stroke and strength are considered. It is worth to recall that
323 the probability of exceedance of the seismic action suggested by the standards for the dampers design
324 is not homogeneous (10% in 50 years for the European codes and 5% in in 50 years for the existing
325 buildings or the MCE for the new ones in the American code). In order to compare results, the same
326 design action has been considered in the parametric analysis. More precisely, the design action has
327 an annual probability of exceedance equal to 2.1×10^{-3} and it coincides with the action suggested by
328 European Standards.

329 In detail, γ_v and γ_Δ denote the amplification factors relevant to velocity and stroke, respectively.
330 The first case analysed, (case $\gamma_v = \gamma_\Delta = 1.0$), considers the response parameters reported in **Table 5**
331 and **Table 6** for the design, without applying any amplification through safety factors. Three more
332 cases are analysed: “ $\gamma_v = 1.5$ and $\gamma_\Delta = 1.0$ ” where the displacement is not amplified, while the force
333 is associated with a velocity equal to $\gamma_v = 1.5$ times the maximum one; “ $\gamma_v = \gamma_\Delta = 1.5$ ” where the
334 displacement is amplified with a coefficient equal to $\gamma_\Delta = 1.5$, while the force is associated with a
335 velocity equal to $\gamma_v = 1.5$ times the maximum one; “ $\gamma_v = \gamma_\Delta = 2.0$ ” where the displacement is
336 amplified with a coefficient equal to $\gamma_\Delta = 2.0$, while the force is associated with a velocity equal to
337 $\gamma_v = 2.0$ times the maximum one.

338 Moreover, one more case is considered that accounts for larger amplification factors: “ $\gamma_v = \gamma_\Delta =$
339 3.0 ” where the displacement is amplified with a coefficient equal to $\gamma_\Delta = 3.0$, while the force is
340 associated with a velocity equal to $\gamma_v = 3.0$ times the maximum one. Finally, for comparison
341 purposes, two more limit cases are considered: “No Failure” that is the case where no dampers’
342 failures are permitted, and “Bare Model”, which represents the frame without FVDs.

343 3.5 Probabilistic framework

344 A conditional probabilistic approach is used to estimate, for each case study, the demand hazard
345 functions $v_D(d)$ of the random variable D describing the main parameters characterizing the seismic
346 response of the structural systems. The stages needed to estimate $v_D(d)$ by a conditional probabilistic
347 approach are: *i*) evaluation of the hazard function $v_{IM}(im)$, i.e., the MAF of exceeding the value im of
348 the intensity measure IM ; *ii*) construction of a probabilistic demand model, expressed by the function
349 $G_{D|IM}(d|im)$, linking the generic demand D with the IM and expressing the probability of exceeding
350 the demand value d conditional to the seismic intensity level im ; *iii*) estimation of the mean annual
351 rate of exceedance $v_D(d)$ by solving the following convolution integral between the seismic hazard
352 function v_{IM} and the conditional demand $G_{D|IM}$.

$$v_D(d) = \int_{IM} G_{D|IM}(d|im) |dv_{IM}| \quad (9)$$

353 In this study, the standard trapezoidal rule is used to solve the integral of Eq. (9), while Multy-
354 Stripes Analysis (MSA) is employed to build the $G_{D|IM}$ function, which requires performing a number
355 (n_{sim}) of nonlinear dynamic structural analyses at discrete IM levels (n_{IM}). In order to achieve accurate
356 risk estimations, the number of IM levels used to perform MSA is set equal to 20, and at each IM
357 level the 30 ground motions with the closest IM values are selected and scaled to that IM level. This
358 approach, yielding different ground motion combinations for the different IM levels considered,
359 permits to avoid excessive scaling of the records. The choice of the values of n_{sim} (30) and n_{IM} (20) is
360 based on the results of a recently proposed study [34], in which an extensive parametric analysis was
361 performed to assess the influence of the main parameters governing MSA on the accuracy of the risk
362 estimates.

363 4 EFFECTS OF FVDS FAILURE ON THE BENCHMARK STRUCTURES RESPONSE

364 Before illustrating the results of the probabilistic analyses in detail, it is useful to provide a first
 365 insight on the dynamic behaviour following the damper failures. FVDs failures are explicitly
 366 modelled based on section 2.1.

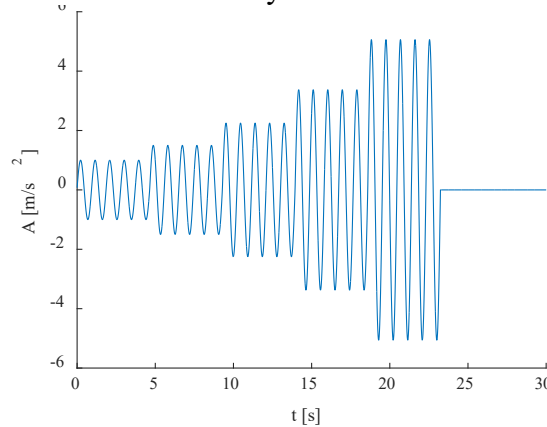
367 In the following, the results obtained for a sinusoidal ground motion of increasing intensity striking
 368 the three-storey building are presented first. Successively, the seismic response is discussed,
 369 considering some ground motions selected from the MSA analysis. Finally, a preliminary and
 370 qualitative evaluation of the overall probabilistic response of the three-storey case-study is proposed.

371 Analysis results highlight some typical issues related to the damper failures, such as the domino
 372 effect on dampers at different storeys, acceleration peaks due to end-stroke impacts, and overall brittle
 373 behaviour of the system.

374 4.1 System response under an increasing sinusoidal input

375 In this subsection, the results obtained for a sinusoidal ground motion of increasing intensity
 376 striking the 3-storey building are presented. The FVDs response parameters at the design condition
 377 refer to linear devices ($\alpha = 1$) and to the case “ $\gamma_v = \gamma_\Delta = 1.0$ ”. The choice of an increasing harmonic
 378 input motion is motivated by the fact that it allows to easily identify the attainment of the damper
 379 strength capacity through one of the two mechanisms, impact and over-velocity and the related
 380 consequences on the frame undergoing a more general time-history input motion.

381 **Fig. 5** shows the sinusoidal input having a period of 0.9 seconds and an initial magnitude of
 382 1 m/s^2 . The amplitude of the motion is constant for five cycles, after that it is increased with a
 383 coefficient equal to 1.5 and remains again constant for five cycles. The magnification of the motion
 384 amplitude is repeated four times, resulting in a motion that has five different amplitudes, with a
 385 maximum equal to 5 m/s^2 , and that lasts 22.5 seconds. At the end of the input, there are few seconds,
 386 which are useful to understand how the case study restores its rest condition.

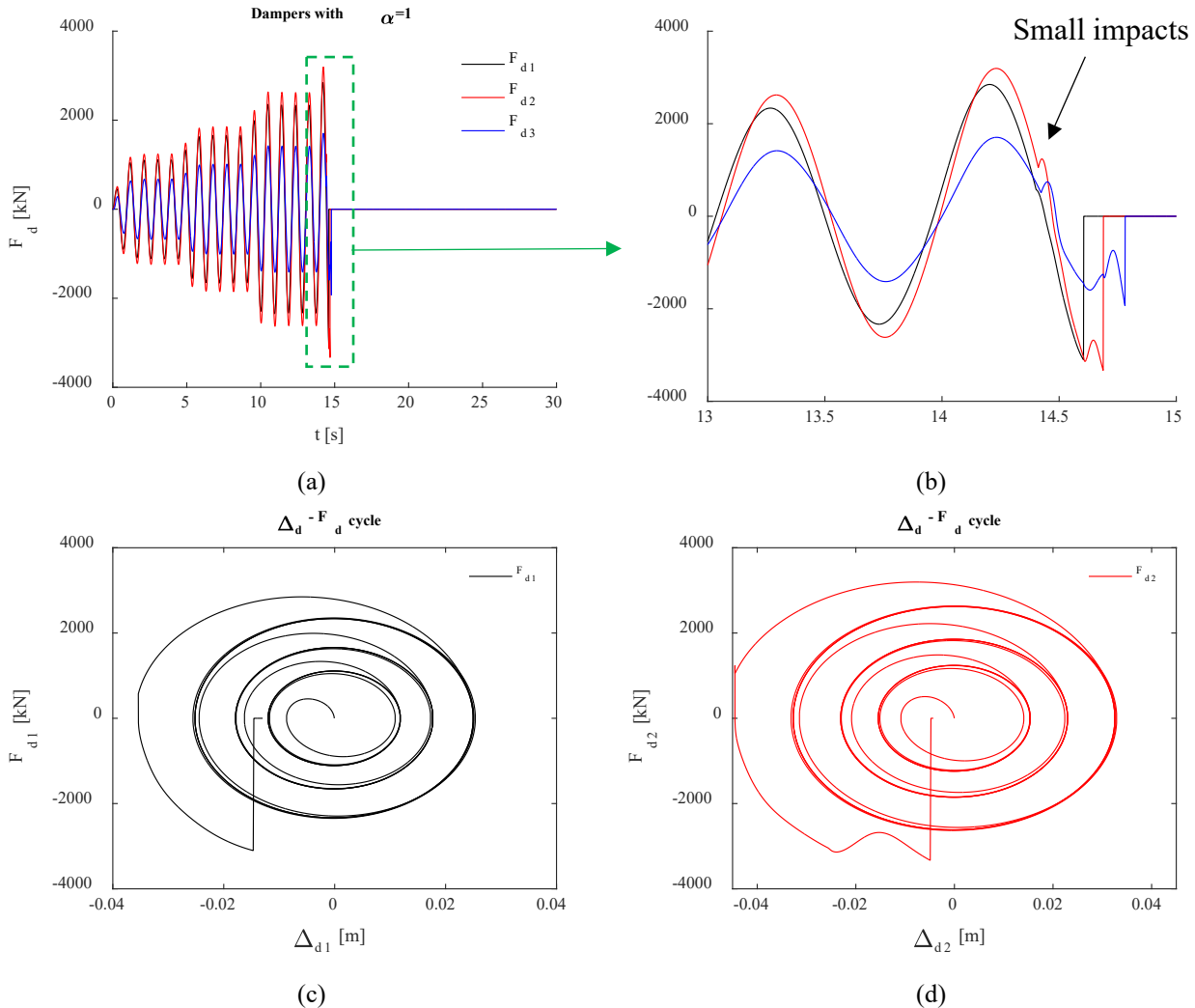


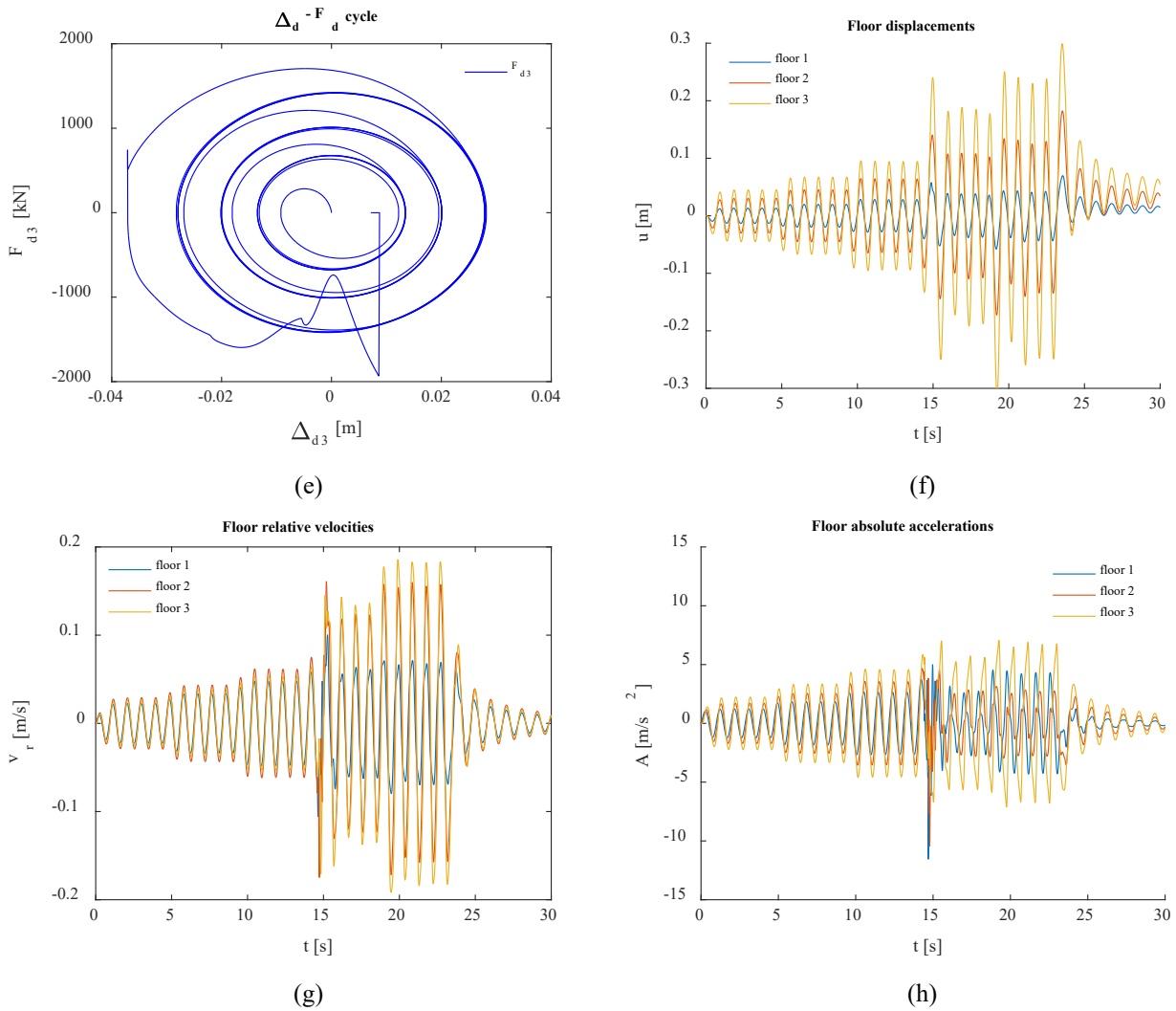
387 **Fig. 5.** Sinusoidal incremental dynamic input

389 **Fig. 6 a) - Fig. 6 h)** show the response in terms of damper forces and strokes, $F_{d,i}$ and $\Delta_{d,i}$. floor
 390 displacements u_i , floor relative velocities $v_{r,i}$ and floor absolute accelerations A_i . In particular, **Fig.**
 391 **6 a)** and **b)** illustrate the time-history of the damper forces $F_{d,i}$ recorded along the height of the
 392 building. The black solid line refers to the device installed between the ground and the first floor, the
 393 red one refers to the intermediate device at the second storey, while the blue one represents the damper
 394 at the top storey. At the beginning of the third increment of the sinusoidal input (between 14.4 and
 395 14.5 seconds), graphs show some small ripples, which are more evident for the intermediate and top-
 396 storey devices (**Fig. 6 b)**), and they are caused by small impacts due to the end-stroke attainment. In
 397 this case, the impact occurs but it does not lead to the attainment of the damper strength capacity. At
 398 the time instant 14.6 s the damper placed at the first level reaches its force capacity due to over-
 399 velocity and its force drops to zero. Few instants later, also the other devices fail for over-velocity.
 400 These effects can be deeper investigated through **Fig. 6 c) - e)**, where the stroke-force relationship of

401 each device is shown. In particular, by observing the stroke-force relationships of Fig. 5 c) - e) it is
 402 evident that at the beginning of the third increment of the input motion, all the three dampers
 403 experience the end-stroke attainment without failure, with impacts that are more evident for the
 404 intermediate and top-storey devices. After these impacts, occurred without consequences, the FVDs
 405 restore their behaviour as pure dissipative devices. Few instants later, suddenly, the damper located
 406 at the ground floor fails due to over-velocity, triggering the sequence of damper failures at the upper
 407 elevations. The sequence is highlighted by a series of ripples in the stroke-force relationship of the
 408 intermediate and especially top-storey device. The ripples begin when the first device fails and last
 409 until all the devices fail for over-velocity.

410 **Fig. 6 f) - h)** shows the time-histories of the parameters strictly related to the frame response,
 411 highlighting the consequences of the damper failures on the frame itself. Generally, the responses in
 412 terms of displacements, relative velocities and absolute accelerations are significantly amplified by
 413 the impacts occurring in the dampers and by their failure. The absolute accelerations are more affected
 414 than the displacements. It is worth to note that the peaks in terms of absolute accelerations, recorded
 415 between 14 and 15 seconds, are mainly related to the impacts experimented by the devices before
 416 their failure.





417 **Fig. 6.** Dampers response and time histories of different local and global EDPs under harmonic
 418 incremental dynamic input

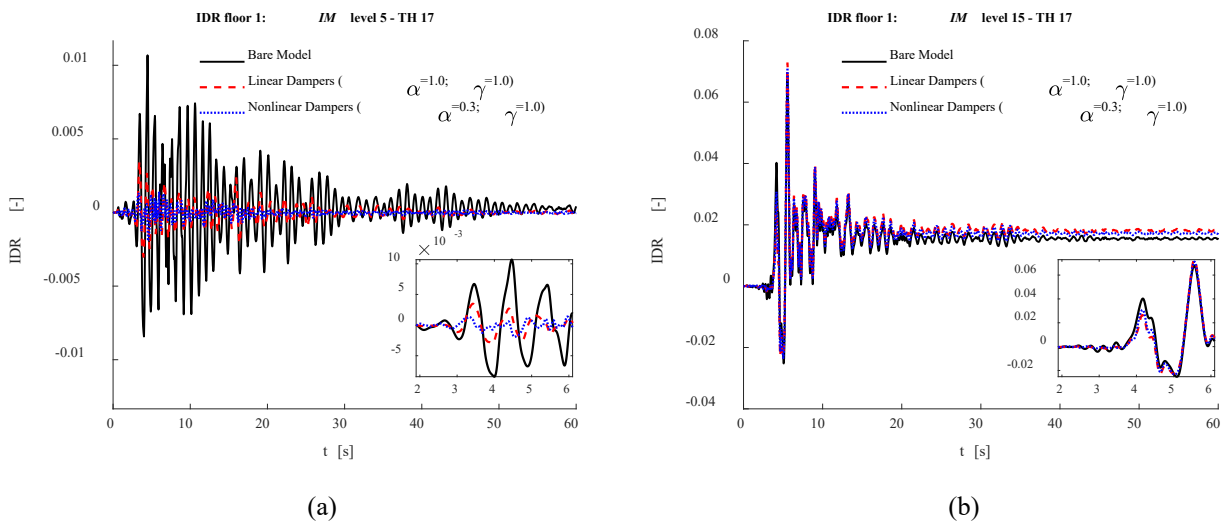
419 **4.2 Three-storey building and nine-storey building seismic response overview**

420 In this subsection, few selected information from MSA analysis are shown to illustrate overall the
 421 problem of damper failure and related effects on the structural performance of the three-storey and
 422 nine-storey building case studies.

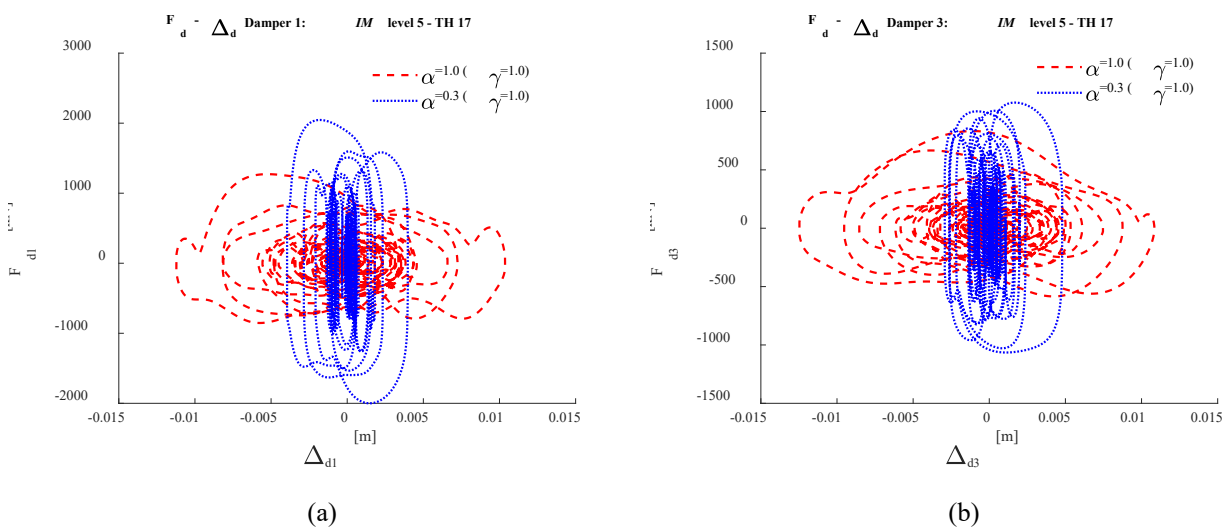
423 To shed further light on the consequences of FVDs failure, the time-histories of the interstorey-
 424 drift ratio (IDR) response of the bare model and of the system with (linear and nonlinear) dampers
 425 designed without amplification factors ($\gamma_v = \gamma_\Delta = 1.0$) are compared in **Fig. 7**. Comparison is
 426 performed at both low (*IM* level 5) and high (*IM* level 15) seismic intensities and for a single time-
 427 history (TH) analysis (TH 17). For sake of brevity and given the high similarity of the response at all
 428 floors the response in terms of IDR at floor 1 is only discussed. It is confirmed that at lower seismic
 429 intensities FVDs are effective in damping the response (by also reducing residual drift) and that the
 430 beneficial response mitigation provided by the dampers vanishes at higher *IM*s, due to the device
 431 failure. More specifically, it can be observed that dampers fail at around 4.0 seconds since the
 432 beginning of the time-history of *IM* level 15. This is detailed in the inset of **Fig. 7** (b) (close-up plot
 433 between 2 and 6 seconds), showing that the IDR response (with both linear and nonlinear devices) is
 434 damped until the 4.0 s and then tends towards the bare-frame response; on the contrary, at *IM* level 5
 435 the response of the frame with FVDs is damped over the whole earthquake duration, since no device
 436 failure is observed at this intensity level.

437 For sake of completeness, the dampers force-stroke cyclic responses corresponding to the
 438 aforesaid cases (plotted in **Fig. 7**) are shown in **Fig. 8** (*IM* level 5) and **Fig. 9** (*IM* level 15). In each
 439 figure a comparison is made between the responses of the linear (red dashed line) and nonlinear
 440 dampers (blue dotted line) at the first (figure a) and third storey (figure b). The attainment of the end-
 441 stroke (impact) is characterised by a sudden rise in force (with no increase of displacement) while the
 442 attainment of the maximum force capacity (hence the failure) can be identified because the force
 443 suddenly becomes null and the hysteretic cycle is interrupted. It can be noted that at *IM* level 5 failure
 444 is never attained, and thus complete cycles can be observed in **Fig. 8**.

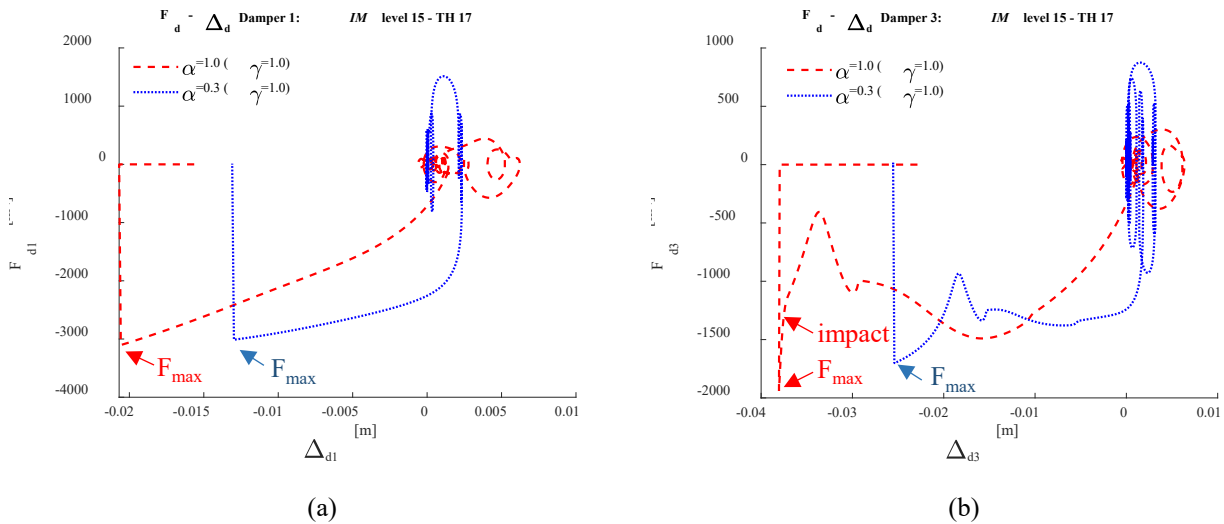
445 On the contrary, at *IM* level 15 failure occurs on the dampers of both storeys 1 (**Fig. 9a**) and 3
 446 (**Fig. 9b**), corresponding to the cycle's sudden interruption. More in detail, in **Fig. 9a** (floor 1) the
 447 failure is achieved with no sign of impact (for both linear and nonlinear dampers); differently, in **Fig.**
 448 **9b** (floor 3), the force of the linear damper (red line) increases abruptly and immediately after drops
 449 to zero, meaning that the impact is responsible for the failure.
 450



451 **Fig. 7.** Time histories of the IDR at two different *IM* levels (a) *IM* n. 5 and (b) 15. Comparison
 452 between the bare model and the model with linear and nonlinear dampers (without amplification
 453 factors).

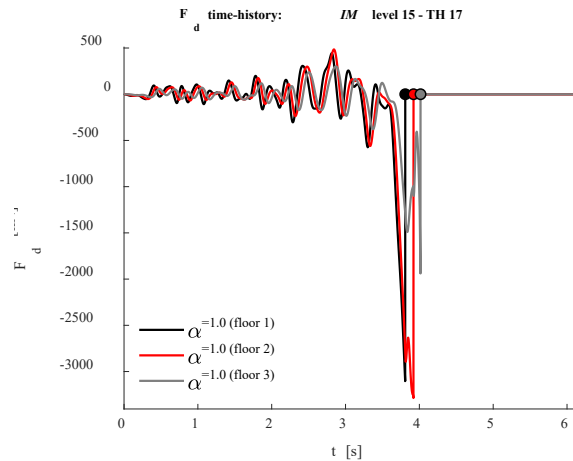


454 **Fig. 8.** Damper response at *IM* levels 5. Comparison between linear and nonlinear dampers
 455 (without amplification factors) at (a) first and (b) third floor.



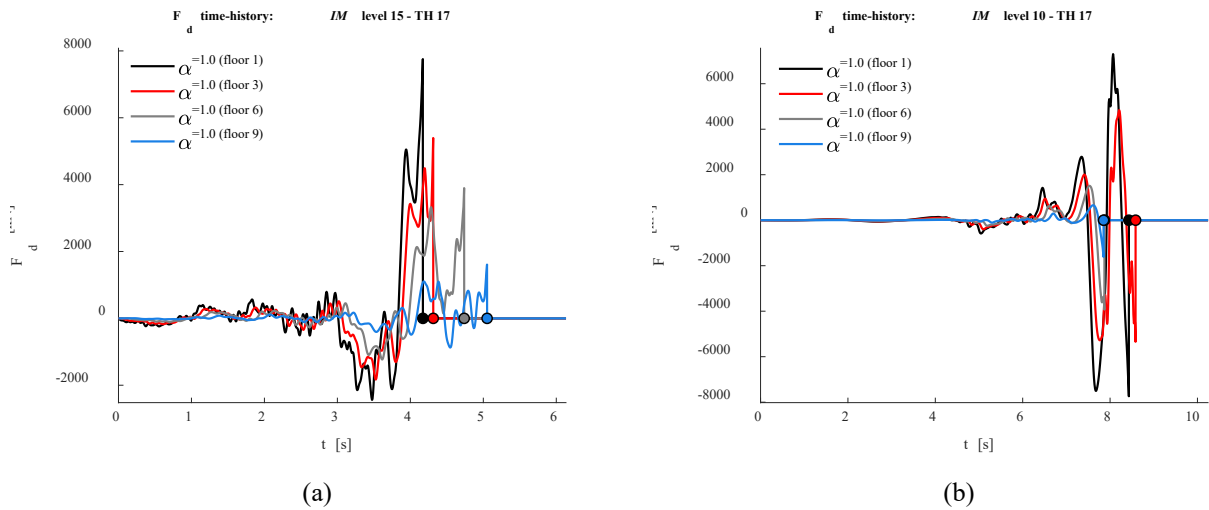
456 **Fig. 9.** Damper response at *IM* levels 15. Comparison between linear and nonlinear dampers
 457 (withouth amplification factors) at (a) first and (b) third floor.

458 In **Fig. 10**, time histories (selected from *IM* level 15) of the force on dampers at different floors
 459 are compared. Here dampers failure occurs at 4.0 s, when the forces suddenly drop to zero and the
 460 dampers become ineffective. It can be also observed that failure involves devices at all the storeys
 461 quite simultaneously.



462 **Fig. 10.** Failure time-lag among dampers at different floors.

464 For what concerns the seismic response of the nine-storey building, the differences between the
 465 seismic response of this structural system and the previous low-rise building are highlighted in the
 466 following. **Fig. 11 a)** shows the time-history of the forces at the various levels under record #17
 467 scaled to the *IM*=15 (with intensity 2.0 g, 2.26 times higher than the design seismic intensity).
 468 Although damper failure initiates at the bottom storey, it propagates quite rapidly to the devices
 469 placed at the higher levels. However, damper failure can also propagate from the top to the bottom
 470 of the building, as observed by the response shown in **Fig. 11 b)**, related to the same record scaled
 471 to *IM*=10 (design seismic intensity). In general, it is observed that when one device fails, all the
 472 other devices fail too, even though at different times.
 473



474 **Fig. 11.** Failure time-lag among dampers at different floors: *IM* level n. 15 (a) and 10 (b) *IM*.

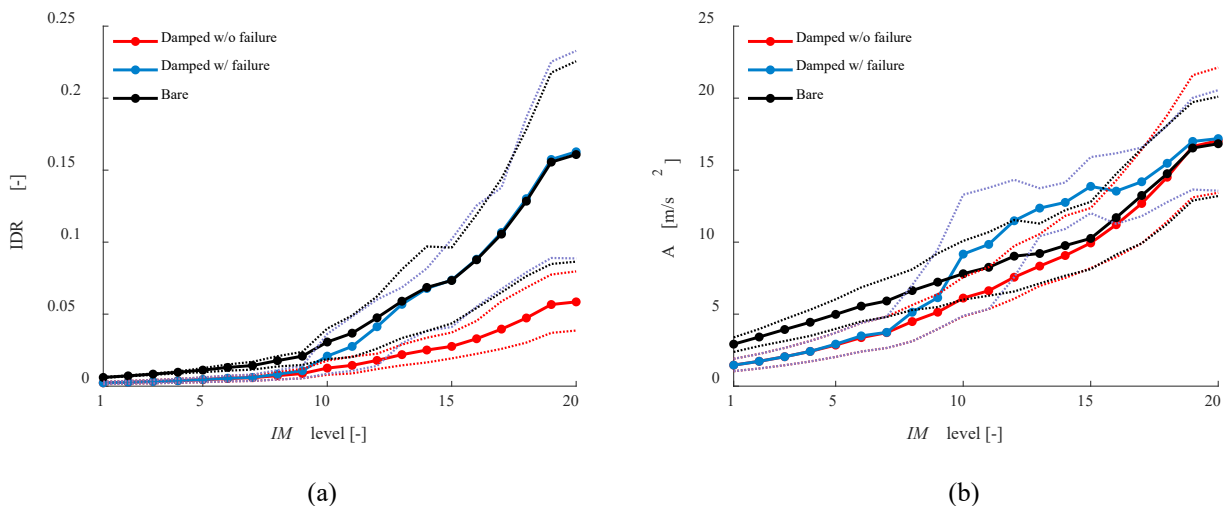
475 **4.3 Qualitative evaluation of the overall probabilistic response**

476 In this section a preliminary evaluation of the overall probabilistic response of the three-storey
 477 building is provided. **Fig. 12** shows the building response in terms of IDR and acceleration at storeys
 478 (A) at different seismic intensities for the case of linear dampers ($\alpha = 1.0$). For each *IM* level, the
 479 median response values are shown by using continuous lines with circle markers, and different
 480 colours are used to compare the following three cases: 1) bare model (black); 2) building with
 481 dampers designed without amplification factors ($\gamma_v = \gamma_\Delta = 1$) (blue); 3) building with dampers with
 482 neither impact nor failure model ($\gamma_v = \gamma_\Delta = \infty$) (red). Moreover, the 16th and 84th percentiles
 483 are plotted by dotted lines by using the same colours described above.

484 The following observations can be made:

- 485 • FVDs without failure significantly reduce the IDR of the building up to the highest seismic
 486 intensities, with a lower beneficial effect in terms of acceleration mitigation;
- 487 • If the device failure is taken into account, the response mitigation provided by the dampers
 488 vanishes for *IM* levels higher than 10, corresponding to design condition (0.8866 g);
- 489 • Once failed, devices are no longer effective and the IDR response of the damped systems
 490 tends to be almost that of the bare building, while the response in acceleration shows peaks
 491 higher than the undamped frame system, due to the impacts induced by the devices end-
 492 stroke attainment.

493 The observations above also apply to the case with nonlinear dampers (not shown due to space
 494 constraints).



495 **Fig. 12.** Building response at different IM levels for the case with linear dampers ($\alpha=1.0$) in terms
496 of (a) IDR and (b) A. Comparison between damped (with and without failure) and bare model.

497 5 PROBABILISTIC ANALYSIS RESULTS: THREE-STOREY BUILDING

498 The performance of the case studies is evaluated by monitoring a wide set of EDPs. To provide
499 information on the damage level of the main structural system, the following global EDPs are
500 considered: the maximum interstorey drift among the various storeys (IDR), the maximum roof drift
501 (RDR), the maximum residual interstorey drift among the storeys (IDR_{res}), and the maximum absolute
502 acceleration at storeys (A). The dampers performance is monitored by considering the following two
503 local EDPs, accounting for the cost, the size and the failure of the devices: the maximum absolute
504 force of the dampers (F_{di}) and the maximum stroke (Δ_{di}).

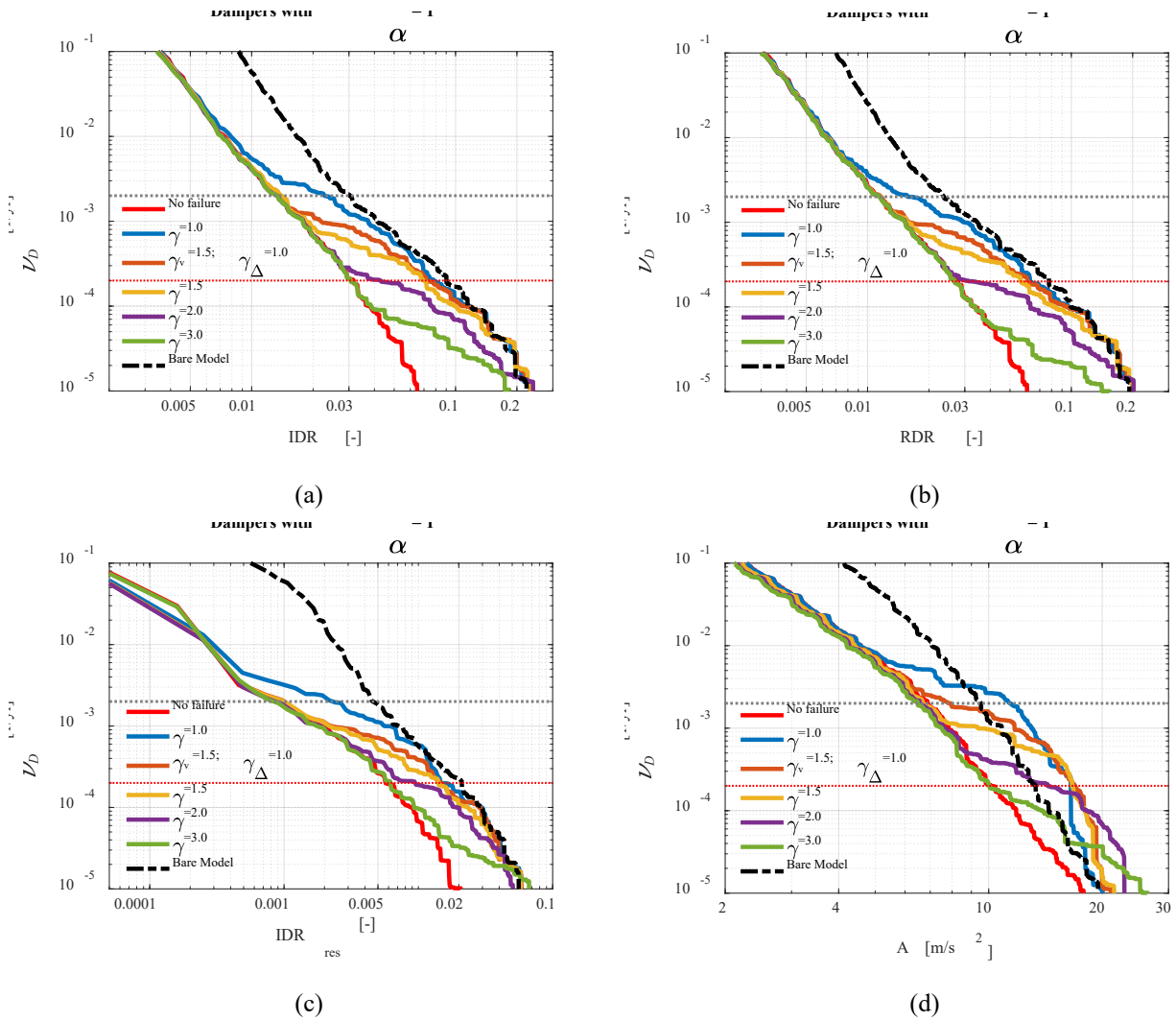
505 5.1 Demand hazard curves

506 This subsection shows the demand hazard curves of all the monitored EDPs, with respect to the
507 mean annual rate of exceedance ν_D , for each damper typology ($\alpha = 1.0, \alpha = 0.6, \alpha = 0.3$).
508 Comparisons are made among the various analysed cases, namely: dampers without amplification
509 factors ($\gamma_v = \gamma_\Delta = 1.0$) (blue solid line) and dampers designed with different γ factors, that is $\gamma_v =$
510 1.5 and $\gamma_\Delta = 1.0$ (brown solid line); $\gamma_v = \gamma_\Delta = 1.5$ (yellow solid line); $\gamma_v = \gamma_\Delta = 2.0$ (violet solid
511 line); $\gamma_v = \gamma_\Delta = 3.0$ (green solid line). Moreover, the demand hazard curve of the following two cases
512 are added for comparison purposes: bare frame model (black dashed line) and damped model without
513 damper failure (i.e., with $\gamma_\Delta = \gamma_v = \infty$) (red solid line). Also, two horizontal dotted lines are depicted
514 in the charts, one identifying the design hazard level 0.0021 yr^{-1} (black dotted line) and the other (red
515 dotted line) denoting the target risk level desired for the structural systems ($2 \times 10^{-4} \text{ yr}^{-1}$) [23].

516 Results concerning the linearly damped building are first presented. The demand hazard curves of
517 the main global EDPs (IDR, RDR, IDR_{res} , A) are illustrated in **Fig. 13**, whereas those concerning the
518 damper response (F_{di} and Δ_{di}) are illustrated in **Fig. 16**. Only the curves of the dampers at floor 1 are
519 shown, given the similarity of the results among the storeys.

520 Based on **Fig. 13** the following comments can be made:

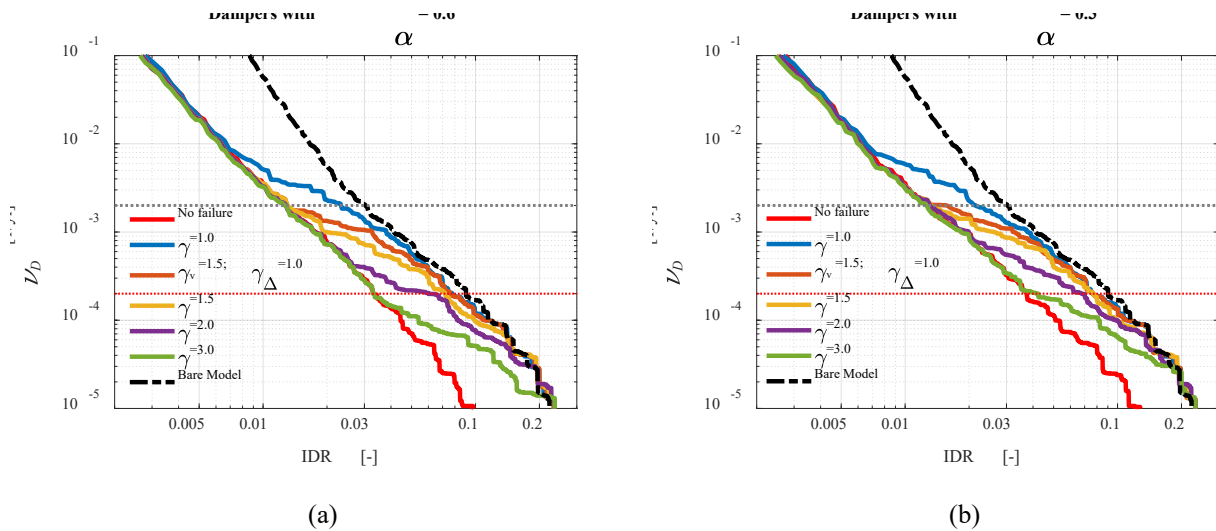
- 521 • For all the cases with dampers and amplification factors larger than 1.0, the rate of exceeding
522 of the target drift performance ($IDR=0.012$) is around 0.0021 yr^{-1} , the hazard level of the design
523 action, represented by the horizontal black dotted line, with some slight deviations that can be
524 justified by the probabilistic nature of the analysis (contribution to the exceedance probability
525 from IM levels different from the reference one [28][29]).
 - 526 • If no amplification is considered ($\gamma_v = \gamma_\Delta = 1$, blue curve), the rate of exceeding of the target
527 drift performance, highlighted by the red dotted line ($IDR=0.012$), is notably higher than the
528 expected one, due to the failures experienced by the dampers at intensity levels lower than the
529 design one (i.e., $IM = 0.89 \text{ g}$) (see Section 5.3 for further details about this point).
 - 530 • Once damper rupture is attained, the building response in terms of maximum and residual drift
531 tends to that of the bare model (black dashed line) and the magnitude of the amplification
532 factors governs the “rapidity” of the transition from the damped to the bare frame curve.
 - 533 • In particular, the IDR, RDR and IDR_{res} approach the bare frame model quite perfectly,
534 conversely, the absolute accelerations, which are lower than those of the bare frame until the
535 dampers are effective, become even higher due to end-strokes impacts experienced by the
536 dampers, before their failures.
 - 537 • The hazard curves of RDR and IDR are very similar and both of them tend to overlap those of
538 the bare model once the dampers fail, meaning that, in this case, the drift demand is uniform
539 along the building height (no soft storey mechanisms have been observed).
- 540



541 **Fig. 13.** Demand hazard curves of the main global EDPs (a) IDR, (b) RDR, (c) IDR_{res}, (d) A for
 542 different damper amplification factors. Case of building with linear dampers ($\alpha = 1.0$).

543 **Fig. 14** shows the IDR demand hazard curves for the cases with nonlinear dampers ($\alpha=0.6$ and
 544 $\alpha=0.3$). The trends are similar to those observed with linear dampers, although there are some
 545 differences worth to be stressed:

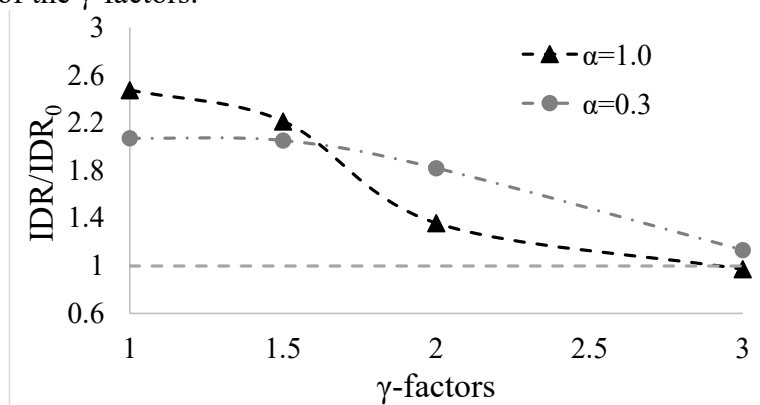
- 546 • The curves of nonlinear dampers have a lower slope, which lead the system to show, for a given
 547 demand value, higher exceedance annual rates. This is consistent with previous studies comparing
 548 the performance of linear and nonlinear FVDs [28].
- 549 • The MAF levels corresponding to the transition from the curve of the damped system to that of
 550 the undamped one are higher for nonlinear dampers compared to the linear ones, and the slope of
 551 such transition increases with the degree of nonlinearity of dampers.



552 **Fig. 14.** Demand hazard curves of the IDR parameter for different damper's amplification factors.
 553 Case of building with nonlinear dampers: (a) $\alpha=0.6$; (b) $\alpha=0.3$.

554 Finally, a deeper discussion is due on the influence of the amplification factors on the structure
 555 reliability (**Fig. 15**). For this purpose, the response corresponding to the reference MAF of 2×10^{-4}
 556 is selected. This value is generally considered as a satisfactory target for the MAF of collapse, as
 557 illustrated in [23][53]. The response corresponding to the reference MAF, in terms of IDR, achieved
 558 for the case where no damper failure is permitted ("No Failure") is assumed as the target response
 559 and identified as IDR_0 . This result is then compared, through the ratio IDR/IDR_0 , with the values of
 560 IDR achieved with four different values of the γ -factors. The analysed cases are $\gamma_v = \gamma_\Delta = 1.0$, that
 561 is dampers without amplification factors and three more cases in which the displacements and the
 562 forces associated with velocities are amplified, that is $\gamma_v = \gamma_\Delta = 1.5$, $\gamma_v = \gamma_\Delta = 2.0$ and $\gamma_v = \gamma_\Delta =$
 563 3.0 .

564 **Fig. 15** shows the variation with γ of the ratio IDR/IDR_0 highlighting that in the case of linear
 565 dampers, the use of a γ -factor equal to 3 permits to obtain the same IDR of the "No failure"
 566 case, whereas in the case of nonlinear devices a value just larger than 1 is reached, ensuring similar
 567 performance in both the linear and nonlinear case. Differently, with lower values of γ -factors,
 568 significantly larger values of the ratio IDR/IDR_0 are obtained, meaning that the response achieved
 569 when accounting for the devices failure is far from the reference one (IDR_0). The trend of the ratio
 570 achieved with linear dampers seems to be more sensible to the variation of the γ -factors, as
 571 highlighted by a change of the slope when γ are comprised between 1.5 and 2. Differently, with
 572 nonlinear devices the trend has a slighter slope, highlighting a value of the ratio IDR/IDR_0 closer to
 573 1 for higher values of the γ -factors.

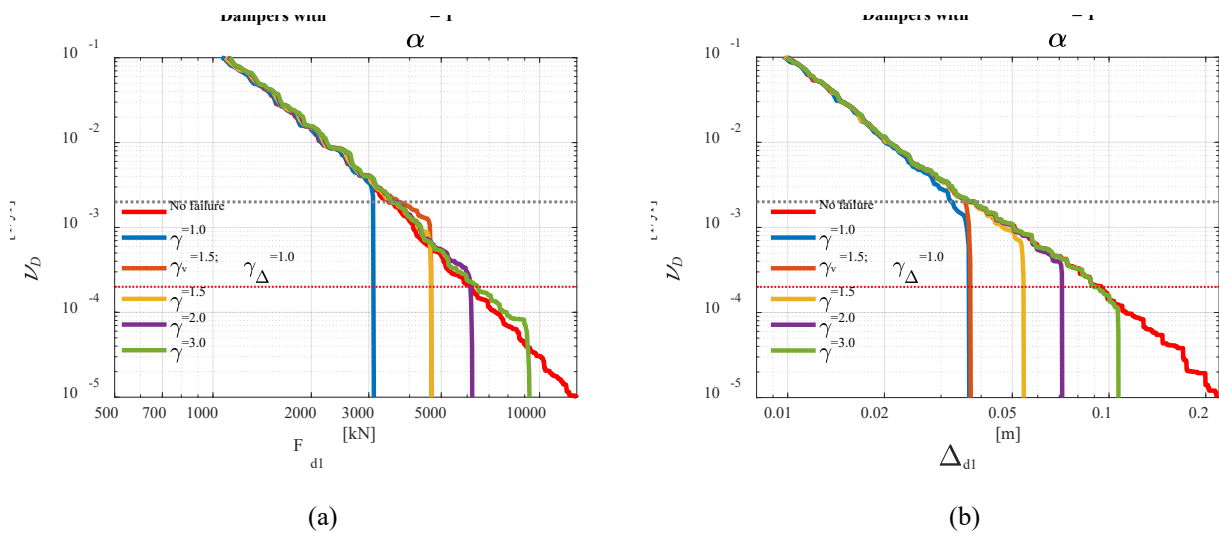


574
 575 **Fig. 15.** Ratios IDR/IDR_0 for different damper amplification factors. Case of building with linear
 576 dampers ($\alpha = 1.0$) and nonlinear dampers ($\alpha = 0.3$).

578 This sub-section examines the demand hazard curves of the EDPs related to the dampers, i.e., the
 579 maximum force and the maximum stroke. **Fig. 16** illustrates the curves of the maximum force (**Fig.**
 580 **16a**) and the maximum stroke (**Fig. 16b**) for the linear damper ($\alpha = 1.0$) at floor n. 1. These are
 581 representative of the outcomes observed at all the floors and the trends observed are the same for all
 582 the types of dampers ($\alpha = 0.6, \alpha = 0.3$). Some general comments on **Fig. 16** follow, which also
 583 apply to all the other cases not displayed in the plots:

- 584 • Dampers designed with $\gamma_v = \gamma_\Delta = 1.0$ (blue curves) fail at a MAF of exceedance higher than
 585 the design hazard level 0.0021 yr^{-1} (black dotted lines), mainly because of over-velocity
 586 phenomena which lead the dampers to attain the ultimate force capacity.
- 587 • Despite the ultimate force capacity is the same, the annual rate of failure for the case $\gamma_v = 1.5$
 588 and $\gamma_\Delta = 1.0$ (brown curves) is higher than the case $\gamma_v = \gamma_\Delta = 1.5$ (yellow curves) due to the
 589 higher number of collapses induced by the end-stroke attainment.
- 590 • All the curves follow the trend of the case with dampers with unlimited capacity (red curves)
 591 until the collapse is attained, then the curves show a sudden vertical drop due to the
 592 impossibility to exceed the ultimate capacity values.

593 **Table 7** to **Table 9** summarise the damper failure rates (v_{fail}) for all the cases analysed, by also
 594 providing the values of $v_{\text{fail}}/v_{\text{target}}$, i.e., the ratios between the actual failure rates and the target risk
 595 levels desired for the structural systems ($2 \times 10^{-4} \text{ yr}^{-1}$) [23]. Ratios higher than one identify cases in
 596 which the target reliability level is not attained, ratios equal or lower than one identify cases in which
 597 the requirement is fulfilled (such values are highlighted by bold font in the tables). It can be observed
 598 that without amplification factors the failure is always attained with a probability higher than the
 599 target one. If the amplification factors are used, the higher the amplification factors, the lower the
 600 $v_{\text{fail}}/v_{\text{target}}$ ratios are. When the amplification factor $\gamma_v = \gamma_\Delta = 3.0$ is applied, the ratios are always
 601 lower than one, except for the nonlinear dampers with $\alpha = 0.3$ at the first and last elevation.
 602



603 **Fig. 16.** Demand hazard curves of the main local EDPs (a) dampers force F_{di} and (b) stroke Δ_{di} for
 604 different damper amplification factors. Case of building with linear dampers ($\alpha = 1.0$).

612

Table 7. Damper failure rates (v_{fail}) and $v_{\text{fail}}/v_{\text{target}}$ ratios of the 3-storey building ($\alpha = 1.0$).

Case of analysis	v_{fail} [1/yr]			$v_{\text{fail}}/v_{\text{target}}$ [-]		
	Floor 1	Floor 2	Floor 3	Floor 1	Floor 2	Floor 3
	$\gamma_{\Delta} = \gamma_v = 1.0$	3.48E-03	3.93E-03	5.45E-03	17.42	19.65
$\gamma_{\Delta} = 1.0$ & $\gamma_v = 1.5$	1.28E-03	1.21E-03	1.54E-03	6.38	6.05	7.70
$\gamma_{\Delta} = \gamma_v = 1.5$	8.80E-04	7.43E-04	1.01E-03	4.40	3.72	5.05
$\gamma_{\Delta} = \gamma_v = 2.0$	2.99E-04	2.57E-04	2.41E-04	1.50	1.29	1.20
$\gamma_{\Delta} = \gamma_v = 3.0$	8.20E-05	3.53E-05	5.41E-05	0.41	0.18	0.27

613

614

Table 8. Damper failure rates (v_{fail}) and $v_{\text{fail}}/v_{\text{target}}$ ratios of the 3-storey building ($\alpha = 0.6$).

Case of analysis	v_{fail} [1/yr]			$v_{\text{fail}}/v_{\text{target}}$ [-]		
	Floor 1	Floor 2	Floor 3	Floor 1	Floor 2	Floor 3
	$\gamma_{\Delta} = \gamma_v = 1.0$	4.08E-03	3.69E-03	4.97E-03	20.39	18.44
$\gamma_{\Delta} = 1.0$ & $\gamma_v = 1.5$	1.68E-03	1.89E-03	1.71E-03	8.38	9.45	8.55
$\gamma_{\Delta} = \gamma_v = 1.5$	1.26E-03	1.33E-03	1.16E-03	6.30	6.65	5.82
$\gamma_{\Delta} = \gamma_v = 2.0$	4.42E-04	4.46E-04	4.28E-04	2.21	2.23	2.14
$\gamma_{\Delta} = \gamma_v = 3.0$	1.54E-04	1.33E-04	1.32E-04	0.77	0.66	0.66

615

616

Table 9. Damper failure rates (v_{fail}) and $v_{\text{fail}}/v_{\text{target}}$ ratios of the 3-storey building ($\alpha = 0.3$).

Case of analysis	v_{fail} [1/yr]			$v_{\text{fail}}/v_{\text{target}}$ [-]		
	Floor 1	Floor 2	Floor 3	Floor 1	Floor 2	Floor 3
	$\gamma_{\Delta} = \gamma_v = 1.0$	4.86E-03	5.21E-03	7.72E-03	24.30	26.07
$\gamma_{\Delta} = 1.0$ & $\gamma_v = 1.5$	2.06E-03	2.04E-03	2.50E-03	10.60	10.22	12.49
$\gamma_{\Delta} = \gamma_v = 1.5$	1.61E-03	1.60E-03	1.94E-03	8.07	8.02	9.70
$\gamma_{\Delta} = \gamma_v = 2.0$	6.27E-04	7.58E-04	8.24E-04	3.14	3.79	4.12
$\gamma_{\Delta} = \gamma_v = 3.0$	2.48E-04	1.81E-04	2.25E-04	1.24	0.91	1.12

617

618

619

620

621

622

623

624

625

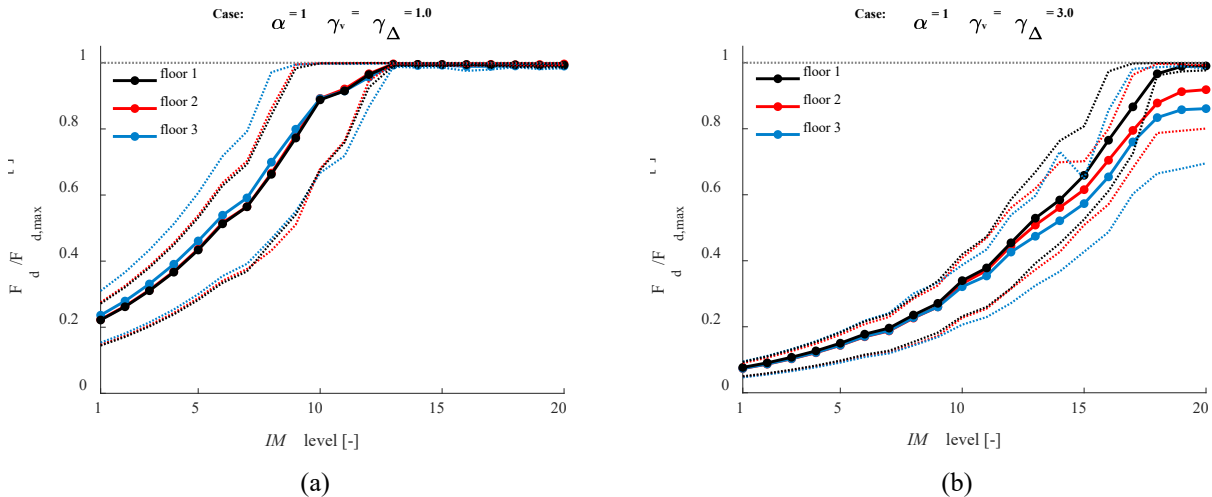
626

627

628

629

Finally, further light is shed regarding the effect of the amplification factors on the sequence of dampers failure among different storeys. For this purpose, it can be useful to refer to **Fig. 17**, where the average trends of the $F_d/F_{d,max}$ ratios are depicted (together with the 16th and 84th response percentiles), for different intensity levels and for all the building storeys. Being all the curves almost perfectly overlapped, it means that there are not cases in which some devices remain active while others fail. The only exception to this general result is represented by the case in which high γ -factors ($\gamma_v = \gamma_{\Delta} = 3$) are used. Indeed, beside the curve shifting towards higher *IMs*, curves of dampers belonging to different floors slightly deviate at the highest seismic intensities, by testifying the presence of few cases in which the dampers at the higher floors do not fail together with the other located at the lower floors. This aspect will be further discussed for the case of the 9-storey building, which shows a higher sensitivity to the γ -factor values. The results obtained for nonlinear dampers are similar to the ones presented here and are not reported due to space constraints.



630 **Fig. 17.** Average and 16th and 84th response percentiles of the $F_d/F_{d,max}$ – IM trends at different
 631 floors for γ factors (a) $\gamma_v = \gamma_\Delta = 1$ and (b) $\gamma_v = \gamma_\Delta = 3$.

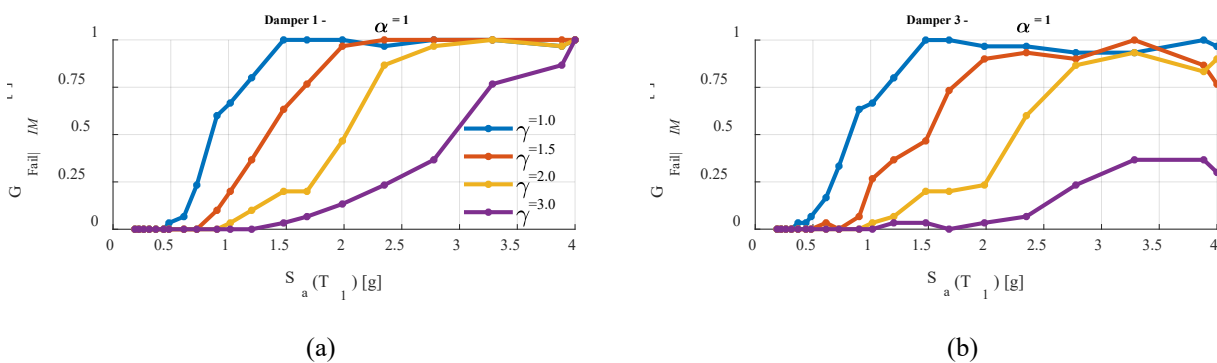
632 **5.3 Dampers collapse fragility functions**

633 In this section, the problem of damper failure is analysed in terms of fragility functions $G_{fail|IM}$,
 634 providing information about the dependency of the probability of failure with the seismic intensity.

635 **Fig. 18** shows the fragility curves of the linear dampers placed at the first and third floor, for all
 636 the different γ -factors analysed.

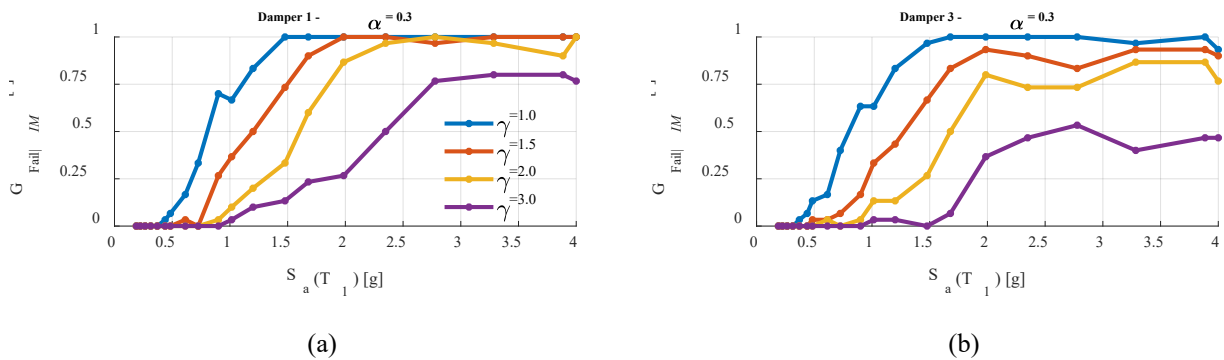
637 Based on these results, the following observations can be made:

- 638 • The absence of amplification factors leads to high damper failure probabilities (>50%) at
 639 seismic intensities lower than the design level (i.e., $IM = 0.89 g$), and from $IM = 1.5 g$ a
 640 100% probability of damper failure is obtained.
- 641 • The beneficial effect of γ -factors larger than 1 is testified by the shifting of the fragility
 642 curves towards higher seismic intensities.
- 643 • Failure probabilities also reduce by moving from floor 1 to floor 3, as can be observed by
 644 comparing the curve of **Fig. 18a** and **Fig. 18b**. However, no differences are observed
 645 among the floors for the case without amplification ($\gamma_v = \gamma_\Delta = 1$).



647 **Fig. 18.** Damper collapse fragility at (a) floor 1 and (b) floor 3 with different amplification factors.
 648 Case of building with linear dampers ($\alpha = 1.0$).

649 Comments above also apply to the case with nonlinear dampers ($\alpha = 0.3$, shown in **Fig. 19**), with
 650 the main exception given by the slightly higher failure probabilities observed in this latter case.
 651



652 **Fig. 19.** Damper collapse fragility at (a) floor n. 1 and (b) floor 3 with different amplification
 653 factors. Case of building with nonlinear dampers ($\alpha=0.3$).

654 6 PROBABILISTIC ANALYSIS RESULTS: NINE-STOREY BUILDING

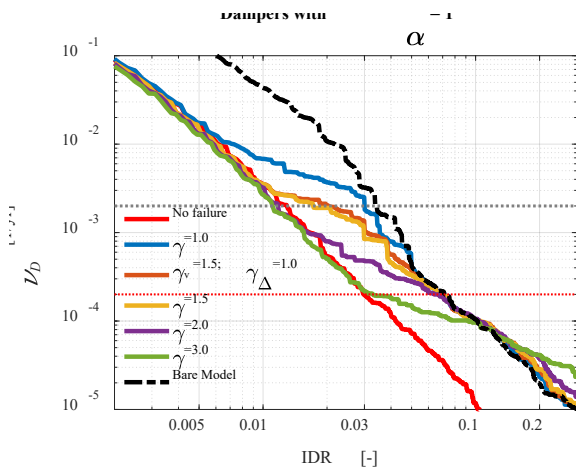
655 This section shows the results concerning the 9-storey building. Due to space constraints, only
 656 selected results are presented. The differences between the seismic response of this structural system
 657 and the previous low-rise building are highlighted, with particular focus on the effect of the
 658 amplification factors on the sequence of dampers failure along the storeys, and the levels of seismic
 659 reliability that are achieved.

660 6.1 Demand hazard curves and failure probabilities

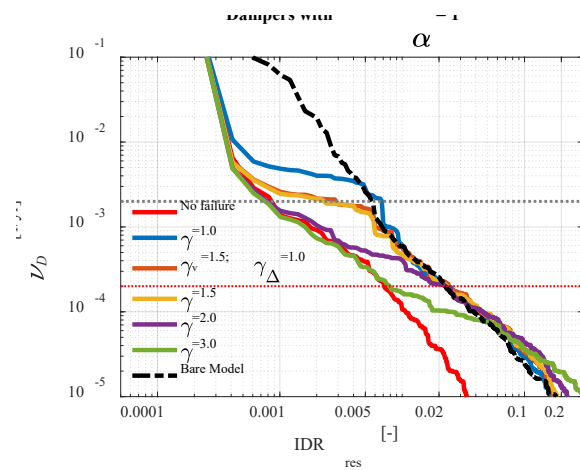
661 **Fig. 20** and **Fig. 21** show the demand hazard curves of the 9-storey building equipped respectively
 662 with linear and nonlinear dampers. In general, the curves follow the same trends observed for the
 663 low-rise system. However, in this case the MAF levels at which the curves start diverging due to
 664 damper failure are notably higher. For instance, the case without amplification factors (blue curve)
 665 deviates from the “no failure” case (red curve) at $v = 10^{-2} \text{ yr}^{-1}$. This is due to the fact that the damper
 666 design is carried out based on the first mode response approximation, which is less accurate for the
 667 medium and high-rise buildings, whose response is significantly influenced by higher-order modes.

668 Moreover, by comparing **Fig. 20** a) and **Fig. 21** a) it is worth noting that the efficiency of the added
 669 dampers reduces for decreasing MAF of exceedances. In fact, higher reductions of drifts are observed
 670 for higher MAF of exceedances than for lower ones, for both the cases of linear and nonlinear
 671 dampers. In this regard, the nonlinear behaviour of the frame (and consequent period-elongation) has
 672 a significant contribution and affects the dampers performance and their efficiency. It is also observed
 673 that the beneficial effect in terms of IDR reduction reduces for increasing levels of nonlinearity of the
 674 dampers (i.e. lower alpha values). In fact, as already highlighted in previous works carried out by the
 675 authors ([28]-[30]), the nonlinear devices are more effective with respect to the linear ones in
 676 controlling the viscous forces, while this efficiency is paid in terms of higher displacements,
 677 particularly for less probable events (lower MAF of exceedance).

678 The use of amplification factors improves the response by shifting the curves towards lower failure
 679 probabilities, as already shown previously for the low-rise building. However, results are worse in
 680 terms of system reliability levels achieved with respect to the 3-storey building.
 681

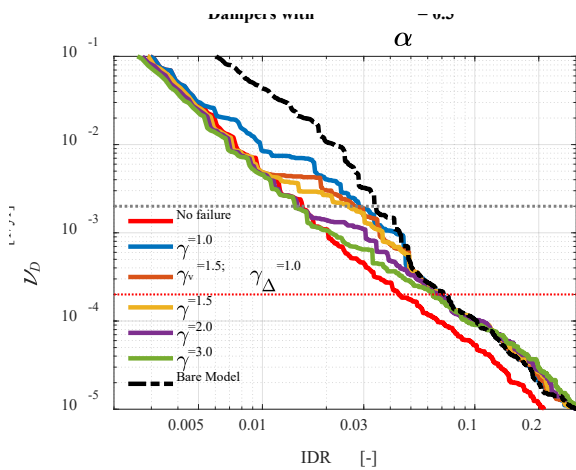


(a)

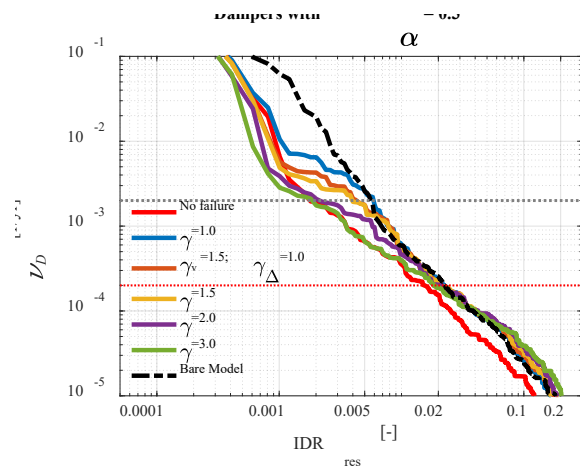


(b)

682 **Fig. 20.** Demand hazard curves of the main global EDPs (a) IDR, (b) IDR_{res} for different damper
 683 amplification factors. Case of building with linear dampers ($\alpha = 1.0$).



(a)

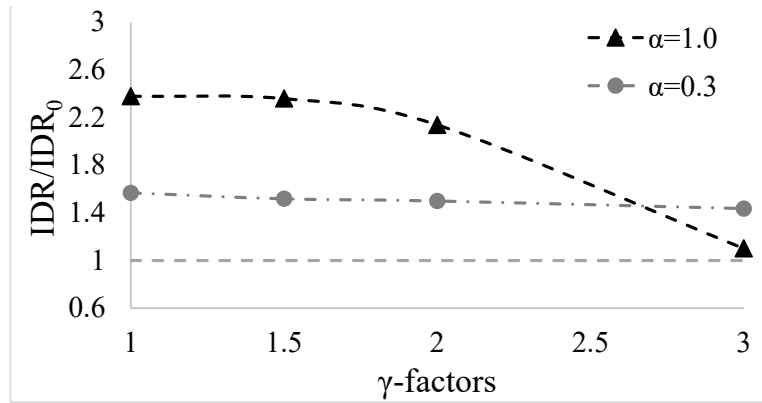


(b)

684 **Fig. 21.** Demand hazard curves of the main global EDPs (a) IDR, (b) IDR_{res} for different damper
 685 amplification factors. Case of building with nonlinear dampers ($\alpha = 0.3$).

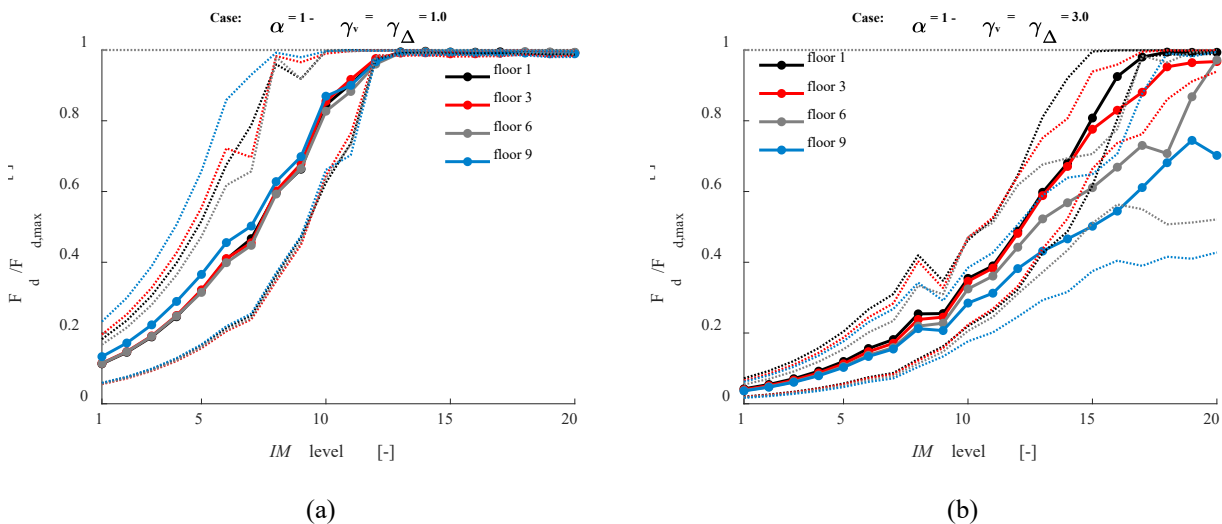
686 As already done for the 3-storey building, with the aim to provide an insight on the influence of
 687 the response amplification factors on the damper failure probability, the IDR response corresponding
 688 to the target MAF of exceedance of 2×10^{-4} is evaluated for different values of γ -factors, and
 689 normalized with respect to the response obtained with dampers that do not suffer failure (IDR₀). **Fig.**
 690 **22** shows the results obtained with γ -factors ranging from 1 to 3 for linear devices ($\alpha=1.0$) and
 691 nonlinear ones ($\alpha=0.3$). It can be observed that, differently from the 3-storey building, the trends
 692 obtained with linear and nonlinear devices are significantly different among them. With linear
 693 dampers, indeed, the use of γ -factors equals to 3 leads nearly to the achievement of the desired
 694 response (IDR₀), ensuring a ratio IDR/IDR₀ slightly higher than one, while lower values of γ -factors
 695 correspond to higher values of the ratio. Differently, the response achieved with nonlinear dampers
 696 seems to be insensitive to change of the γ -factors, with a ratio IDR/IDR₀ that always remains
 697 comprised between 1.56 and 1.43.

698



699 **Fig. 22.** Ratios IDR/IDR₀ for different damper's amplification factors. Case of building with linear
700 dampers ($\alpha = 1.0$) and nonlinear dampers ($\alpha = 0.3$).

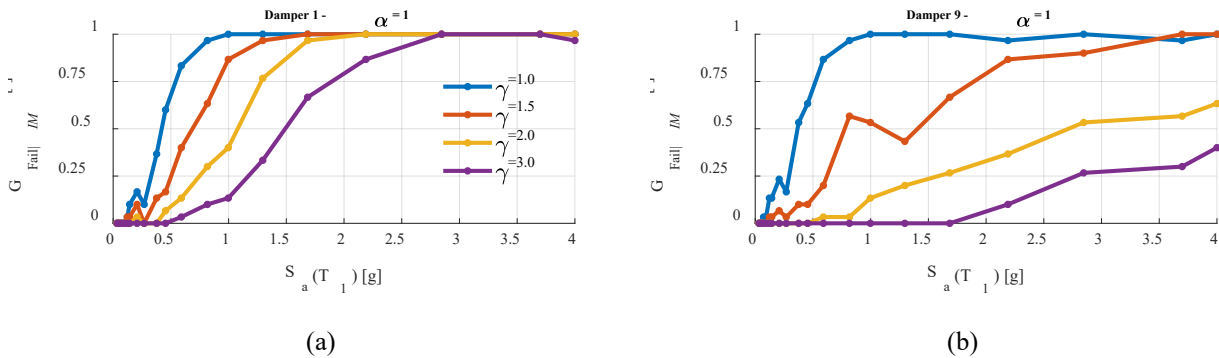
701 Regarding the effect of the amplification factors on the sequence of dampers failure, some further
702 details are provided in **Fig. 23**, as already done for the 3-storey building. In general, it is observed
703 that when one device fails, all the other devices fail too, even though at different times. However, this
704 not always true, and in order to analyse this issue it can be useful to refer to **Fig. 23**, where the average
705 trends of the $F_d/F_{d,max}$ ratios are depicted, for different intensity levels and for different building
706 storeys (i.e., floors n. 1, 3, 6, 9). When no amplification factors are used ($\gamma_v = \gamma_\Delta = 1$), the curves
707 are almost perfectly overlapped (**Fig. 23 a**), thus there are not cases in which some devices remain
708 active while others fail. The response changes if higher γ -factors are used, as shown in **Fig. 23 b**
709 ($\gamma_v = \gamma_\Delta = 3$). Indeed, beside the curve shifting towards higher IMs, curves of dampers belonging to
710 the upper floors slightly deviate at the highest seismic intensities, by testifying a lower average rate
711 of failures, and thus a concentration of collapse cases in the dampers at the lower floors. It is
712 noteworthy that the damage concentration on the structural elements at the storeys with failed
713 (inactive) dampers results in a building performance worse than the one of the bare frame case, this
714 result can be also related to the design method used for the FVDs, which disregards higher order
715 modes.
716



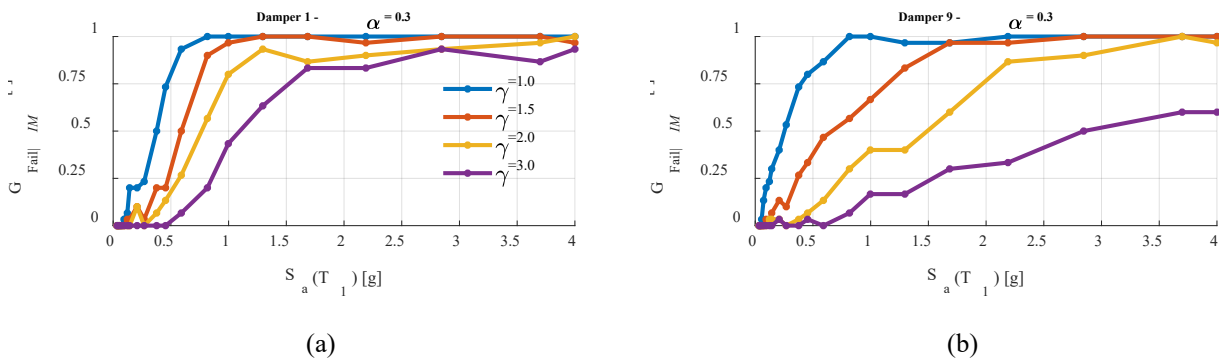
717 **Fig. 23.** Average and 16th and 84th response percentiles of the $F_d/F_{d,max}$ – IM trends at different
718 floors for linear dampers with (a) $\gamma_v = \gamma_\Delta = 1$ and (b) $\gamma_v = \gamma_\Delta = 3$.

719 The damper reliability is also analysed by showing in **Fig. 24** and **Fig. 25** the fragility functions
720 for, respectively, the linear and nonlinear dampers placed at different floors, for the different γ -factors
721 analysed. The results shown in these figures are very similar to those obtained for the 3-floors building
722 (**Fig. 18** and **Fig. 19**). However, in this case the differences between the fragilities of dampers placed

723 at different floors is more evident, thus confirming that a more specialized design method for the
 724 FVDs or different amplification factors at different floors should be used in order to obtain a uniform
 725 failure among dampers of different storeys, as already observed previously.
 726



727 **Fig. 24.** Damper collapse fragility at (a) floor 1 and (b) 9, with and without amplification factors.
 728 Case of building with linear dampers ($\alpha = 1.0$).



729 **Fig. 25.** Damper collapse fragility at (a) floor 1 and (b) 9, with and without amplification factors.
 730 Case of building with nonlinear dampers ($\alpha = 0.3$).

731 **7 CONCLUSIONS**

732 The seismic design of Fluid Viscous Dampers (FVDs) for enhancing the performance of buildings
 733 should ensure proper safety margins against their collapse, and the reliability of the whole structural
 734 system is strongly influenced by the reliability of these devices. Seismic standards generally prescribe
 735 that that the FVDs must be designed based on values of the response parameters (i.e., stroke and
 736 velocity) evaluated at the design condition and amplified by safety factors (reliability factors), in
 737 order to reach a target level of safety. However, the values of these reliability factors are not
 738 homogenous among the various codes and the level of safety attainable through their use has not been
 739 sufficiently investigated.

740 The present paper investigates the issue through the analysis of two benchmark case studies
 741 consisting of a low-rise and a medium-rise steel building equipped with FVDs. A wide range of safety
 742 factor values is considered for the damper design, considering suggestions from international seismic
 743 codes (EN15129 and ASCE-41). A wide parametric investigation is carried out to explore the
 744 influence of these safety factors on both the fragility and the seismic risk of the whole structural
 745 system. The effect of damper nonlinearity is also taken into account analysing damper velocity
 746 exponents ranging from 0.3 to 1.0. The damper shows a brittle failure when its internal force attains
 747 the device strength and this may occur for two reasons: impact when end-stroke is attained, or
 748 attainment of excessive velocity. Both these failure modalities are described by the structural model
 749 and considered in the analyses.

750 As a general result, it is observed that combined effects of impacts and extreme velocities may
751 induce a global brittle behaviour that cannot be perceived by models neglecting these phenomena.
752 More specifically, based on the outcomes of the present study, the following conclusions can be
753 drawn:

- 754 • The consequences of the damper failure on the performance of the whole structural system
755 depend on the number of dampers remained active: if all dampers fail together, then the
756 system response tends to that of the bare building, however absolute accelerations may be
757 higher as a consequence of impacts and dissipation concentrated at some storeys only may
758 leads to a worse global response.
- 759 • The likelihood of the damper failure as well as the “rapidity” of the response transition
760 from damped to bare (or partially damped) structural system are governed by the
761 magnitude of the two amplification factors (γ_{Δ} , γ_v) adopted for damper stroke and velocity.
- 762 • If no amplification is provided ($\gamma_v = \gamma_{\Delta} = 1.0$), the dampers probability of failure is higher
763 than the design hazard level (assumed equal to 0.0021 yr^{-1} in this work), thus, dampers
764 experience failure at intensity levels lower than the design one.
- 765 • The use of amplification factors higher than 1.0 allows attaining lower failure probabilities,
766 and this beneficial effect is more significant for larger γ -factors.
- 767 • Nonlinear dampers ($\alpha=0.3$) exhibit higher failure probabilities (about two times) than the
768 linear ones; moreover, the transition from the damped response (active devices) to that of
769 the undamped one (failed devices) increases at a faster rate increasing the degree of damper
770 nonlinearity.
- 771 • In tall buildings where a design method disregarding higher order modes is used for FVDs,
772 non-uniform failures among dampers of different storeys may occur.

773 Based on the study results, some suggestions can be proposed for further improvements of the
774 design prescriptions of the main international seismic codes. First of all, it should be observed that
775 γ -factors equal to 3, both for stroke and velocity, generally ensure that the target failure probability
776 $2 \times 10^{-4} \text{ yr}^{-1}$ is achieved, despite they might result inadequate in case of dampers with strong nonlinear
777 behaviour (i.e., $\alpha = 0.3$ or lower). Such result, also observed in the 9-storey building, confirms the
778 need of extending the study to γ -factors higher than 3.0. Additionally, the study outcomes suggest
779 that in the case of medium and high-rise buildings, different γ -factors should be employed at the
780 various storeys, and they should be tailored to the specific damper properties present at each storey.
781 It might be also worth to investigate the problem of γ -factors by analysing more closely the
782 damage/plasticity evolution and distribution over the structural elements when devices fail.
783 Moreover, it should be observed that the choice of γ -factors depends on the ratio between the MAF
784 of exceedance chosen for the seismic design action and the target MAF of failure. For example, ASCE
785 code suggests lower MAF for seismic design actions and relevant γ -factors seem to be in line with
786 suggested target value of MAF of failure.

787 It is also worth to note that the amplification of the damper velocity only, without a corresponding
788 amplification of the damper stroke (i.e., $\gamma_{\Delta} = 1.0$ and $\gamma_v > 1.0$), as allowed by the European code
789 EN15129, does not provide significant beneficial effects because the impacts due to the end-stroke
790 attainment makes the effect of γ_v useless. Thus, homogeneous amplification factors (i.e., $\gamma_{\Delta} = \gamma_v$)
791 should be used to achieve a reliable and effective design of FVDs.

792 Given the relevance of these aspects, the extension of the study to a wider range of buildings
793 typologies and design methods will be considered in future works.

794 REFERENCES

- 795 [1] Tubaldi, E., Gioiella, L., Scozzese, F., Ragni, L., & Dall'Asta, A. (2020). A design method for viscous dampers
796 connecting adjacent structures. *Frontiers in Built Environment*, 6, 25.
- 797 [2] Barroso LR. Performance evaluation of vibration controlled steel structures under seismic loads. PhD thesis, Stanford
798 University, California, US, 1999.

- 799 [3] Pavlou, E, Constantinou, M.C., 2006. Response of Nonstructural Components in Structures with Damping Systems,
800 *Journal of Structural Engineering*, **132**(7), 1108-1117.
- 801 [4] Lavan, O, Dargush, G.F., 2009. Multi-Objective Evolutionary Seismic Design with Passive Energy Dissipation
802 Systems, *Journal of Earthquake Engineering*, **13**(6), 758-790.
- 803 [5] Gioiella, L., Tubaldi, E., Gara, F., Dezi, L., Dall'Asta, A. (2018). Modal properties and seismic behaviour of buildings
804 equipped with external dissipative pinned rocking braced frames. *Engineering Structures*, **172**.
805 <https://doi.org/10.1016/j.engstruct.2018.06.043>
- 806 [6] Pavia, A., Scozzese, F., Petrucci, E., & Zona, A. (2021). Seismic Upgrading of a Historical Masonry Bell Tower
807 through an Internal Dissipative Steel Structure. *Buildings*, **11**(1), 24.
- 808 [7] Gioiella, L., Tubaldi, E., Gara, F., Dezi, L., Dall'Asta, A. (2018). Stochastic Seismic Analysis and Comparison of
809 Alternative External Dissipative Systems. *Shock and Vibrations*, **47**. <https://doi.org/10.1155/2018/5403737>
- 810 [8] Tubaldi, E. (2015). Dynamic behavior of adjacent buildings connected by linear viscous/viscoelastic
811 dampers. *Structural Control and Health Monitoring*, **22**(8), 1086-1102.
- 812 [9] Hwang, JS., Lin, WC., Wu, NJ. (2010). Comparison of distribution methods for viscous damping coefficients to
813 building. *Structure and Infrastructure Engineering: Maintenance, Management, Life-Cycle Design and*
814 *Performance*, **9**(1), 28-41. <http://dx.doi.org/10.1080/15732479.2010.513713>
- 815 [10] Silvestri, S., Palermo, M., & Trombetti, T. (2018). A direct procedure for the seismic design of frame structures with
816 added viscous dampers. *Seismic Resistant Structures*, **37**.
- 817 [11] Tubaldi, E., Barbato, M., Dall'Asta, A., 2015. Efficient approach for the reliability-based design of linear damping
818 devices for seismic protection of buildings. *ASCE-ASME Journal of Risk and Uncertainty in Engineering Systems*,
819 *Part A: Civil Engineering*, **2**(2), C4015009. DOI: 10.1061/AJRUA6.0000858.
- 820 [12] Palermo, M., Silvestri, S., Landi, L., Gasparini, G., & Trombetti, T. (2018). A "direct five-step procedure" for the
821 preliminary seismic design of buildings with added viscous dampers. *Engineering Structures*, **173**, 933-950.
- 822 [13] Altieri, D., Tubaldi, E., De Angelis, M., Patelli, E., & Dall'Asta, A. (2018). Reliability-based optimal design of
823 nonlinear viscous dampers for the seismic protection of structural systems. *Bulletin of Earthquake*
824 *Engineering*, **16**(2), 963-982.
- 825 [14] Pollini, N., Lavan, O., & Amir, O. (2018). Optimization-based minimum-cost seismic retrofitting of hysteretic frames
826 with nonlinear fluid viscous dampers. *Earthquake Engineering & Structural Dynamics*, **47**(15), 2985-3005.
- 827 [15] De Domenico, D., Ricciardi, G., & Takewaki, I. (2019). Design strategies of viscous dampers for seismic protection
828 of building structures: a review. *Soil Dynamics and Earthquake Engineering*, **118**, 144-165.
- 829 [16] Victorsson, V.K. (2011). The reliability of capacity-designed components in seismic resistant systems. *PhD thesis*,
830 Stanford University, California, US.
- 831 [17] Tirca, L. and Chen, L. (2014). Numerical simulation of inelastic cyclic response of HSS braces upon fracture.
832 *Advanced Steel Construction*, **10**(4), 442-462.
- 833 [18] Matsui, R., Takeuchi, T., Urui, S., & Tokuno, M. (2018). Collapse Analysis of Steel Frames Considering Fracture of
834 Braces and End of Beams. In *Key Engineering Materials* (Vol. 763, pp. 686-693). Trans Tech Publications.
- 835 [19] American Society of Civil Engineers. Seismic Evaluation and Retrofit of Existing Buildings: ASCE Standard
836 ASCE/SEI 41-17. American Society of Civil Engineers, 2017.
- 837 [20] European Committee for Standardization. EN 15129:2010 - Antiseismic devices, Brussels, Belgium, 2010
- 838 [21] European Committee for Standardization. Eurocode 8-Design of Structures for Earthquake Resistance. Part 1:
839 General Rules, Seismic Actions and Rules for Buildings, Brussels, Belgium, 2004.
- 840 [22] ASCE (American Society of Civil Engineers). (2010). Minimum design loads for buildings and other
841 structures. *Standard ASCE/SEI 7-10*.
- 842 [23] Fajfar, P. (2018). Analysis in seismic provisions for buildings: past, present and future. *Bulletin of Earthquake*
843 *Engineering*, **16**, 2567-2608. DOI: 10.1007/s10518-017-0290-8
- 844 [24] Seo, C.Y., Karavasilis, T.L., Ricles, J.M., Sause, R., 2014. Seismic performance and probabilistic collapse resistance
845 assessment of steel moment resisting frames with fluid viscous dampers, *Earthquake Engineering and Structural*
846 *Dynamics*, **43**(14), 2135-2154.
- 847 [25] Gidaris, I., Taflanidis, A.A., 2015. Performance assessment and optimization of fluid viscous dampers through life-
848 cycle cost criteria and comparison to alternative design approaches. *Bulletin of Earthquake Engineering*, **13**, 1003-
849 1028.
- 850 [26] Tubaldi, E., Barbato, M., Dall'Asta, A., 2014. Performance-based seismic risk assessment for buildings equipped
851 with linear and nonlinear viscous dampers. *Engineering Structures*, **78**, 90-99.
- 852 [27] Tubaldi, E., Kougioumtzoglou, I.A., 2015. Nonstationary stochastic response of structural systems equipped with
853 nonlinear viscous dampers under seismic excitation. *Earthquake Engineering and Structural Dynamics*, **44**(1): 121-
854 138.
- 855 [28] Dall'Asta, A., Tubaldi, E., Ragni, L., 2016. Influence of the nonlinear behaviour of viscous dampers on the seismic
856 demand hazard of building frames. *Earthquake Engineering and Structural Dynamics*, **45**(1), 149-169.
- 857 [29] Tubaldi, E., Ragni, L., Dall'Asta, A., 2015. Probabilistic seismic response assessment of linear systems equipped
858 with nonlinear viscous dampers. *Earthquake Engineering & Structural Dynamics*, **44** (1), 101-120.
859 DOI: 10.1002/eqe.2461

- 860 [30] Dall'Asta, A., Scozzese, F., Ragni, L., Tubaldi, E., 2017. Effect of the damper property variability on the seismic
861 reliability of linear systems equipped with viscous dampers. *Bulletin of Earthquake Engineering*, 15(11), 5025-5053.
862 DOI 10.1007/s10518-017-0169-8
- 863 [31] Lavan, O., Avishur, M., 2013. Seismic behavior of viscously damped yielding frames under structural and damping
864 uncertainties. *Bulletin of Earthquake Engineering*, 11(6), 2309–2332.
- 865 [32] Scozzese, F., Dall'Asta, A., Tubaldi, E., 2019. Seismic risk sensitivity of structures equipped with anti-seismic
866 devices with uncertain properties, *Structural Safety*, 77, 30-47.
- 867 [33] Miyamoto, H. K., Gilani, A. S., Wada, A., & Ariyaratana, C. (2010). Limit states and failure mechanisms of viscous
868 dampers and the implications for large earthquakes. *Earthquake Engineering & Structural Dynamics*, 39, 1279-1297.
- 869 [34] Miyamoto, H. K., Gilani, A. S., Wada, A., & Ariyaratana, C. (2010). Collapse risk of tall steel moment frame
870 buildings with viscous dampers subjected to large earthquakes: PART I: DAMPER LIMIT STATES AND FAILURE
871 MODES OF 10-STOREY ARCHETYPES. *The Structural Design of Tall and Special Buildings*, 19(4), 421-438.
- 872 [35] Lee, D., & Taylor, D. P. (2001). Viscous damper development and future trends. *The Structural Design of Tall*
873 *Buildings*, 10(5), 311-320.
- 874 [36] Agrawal, A. K., & Amjadian, M. (2016). Seismic component devices. In *Innovative bridge design handbook* (pp.
875 531-553). Butterworth-Heinemann.
- 876 [37] Filiatrault, A., & Christopoulos, C. (2006). Principles of passive supplemental damping and seismic isolation.
- 877 [38] Impollonia, N., & Palmeri, A. (2018). Seismic performance of buildings retrofitted with nonlinear viscous dampers
878 and adjacent reaction towers. *Earthquake Engineering & Structural Dynamics*, 47(5), 1329-1351.
- 879 [39] Miyamoto, H. K., Gilani, A. S., Wada, A., & Ariyaratana, C. (2011). Identifying the collapse hazard of steel special
880 moment-frame buildings with viscous dampers using the FEMA P695 methodology. *Earthquake Spectra*, 27(4),
881 1147-1168.
- 882 [40] Vamvatsikos, D., & Cornell, C. A. (2002). Incremental dynamic analysis. *Earthquake Engineering & Structural*
883 *Dynamics*, 31(3), 491-514.
- 884 [41] Scozzese, F., Tubaldi, E., & Dall'Asta, A. (2020). Assessment of the effectiveness of Multiple-Stripe Analysis by
885 using a stochastic earthquake input model. *Bulletin of Earthquake Engineering*, 1-37.
- 886 [42] Barroso LR, Winterstein S. Probabilistic seismic demand analysis of controlled steel moment-resisting frame
887 structures. *Earthquake Engineering and Structural Dynamics* 2002; 31(12):2049–2066.
- 888 [43] Constantinou, M. C., & Symans, M. D. (1992). *Experimental and analytical investigation of seismic response of*
889 *structures with supplemental fluid viscous dampers*. Buffalo, NY: National Center for earthquake engineering
890 research.
- 891 [44] McKenna, F. (2011). OpenSees: a framework for earthquake engineering simulation. *Computing in Science &*
892 *Engineering*, 13(4), 58-66.
- 893 [45] NTC 2018 (2018). Aggiornamento delle “Norme Tecniche per le costruzioni” (in italian). D:M: 17/01/2018 Ministry
894 of Infrastructure and Transport.
- 895 [46] Ohtori, Y., Christenson, R.E., Spencer Jr., B.F. and Dyke, S.J. (2004). Benchmark Control Problems for Seismically
896 Excited Nonlinear Buildings. *Journal of Engineering Mechanics*, 130, 366-385.
- 897 [47] Scozzese F, Terracciano G, Zona A, Della Corte G, Dall'Asta A, Landolfo R. Analysis of seismic non-structural
898 damage in single-storey industrial steel buildings. *Soil Dyn Earthq Eng* 2018; 114:505–19.
899 doi:10.1016/j.soildyn.2018.07.047.
- 900 [48] Scozzese, F., Terracciano, G., Zona, A., Corte, G. D., Dall'Asta, A., & Landolfo, R. (2018). Modeling and seismic
901 response analysis of Italian code-conforming single-storey steel buildings. *Journal of Earthquake*
902 *Engineering*, 22(sup2), 2104-2133.
- 903 [49] Bradley BA. A comparison of intensity-based demand distributions and the seismic demand hazard for seismic
904 performance assessment. *Earthquake Engineering and Structural Dynamics* 2013; 42(15):2235–2253.
- 905 [50] Occhiuzzi A. Additional viscous dampers for civil structures: analysis of design methods based on effective
906 evaluation of modal damping ratios. *Eng Struct* 2009;31(5):1093–101.
- 907 [51] Seleemah, A.A. and Constantinou, M.C. (1997). *Investigation of seismic response of buildings with linear and*
908 *nonlinear fluid viscous dampers*. Report No. NCEER-97-0004. New York: National Center for Earthquake
909 Engineering Research, State University of New York at Buffalo.
- 910 [52] Hanson, R.D. and Song, T.T. (2001). *Seismic design with supplemental energy dissipation devices*. Oakland,
911 California: Earthquake Engineering Research Institute.
- 912 [53] Gkimpraxis, A., Tubaldi, E. & Douglas, J. *Comparison of methods to develop risk-targeted seismic design maps*. *Bull*
913 *Earthquake Eng* 17, 3727–3752 (2019). <https://doi.org/10.1007/s10518-019-00629-w>
914